The Role of Continental Topography in the Present-Day Ocean's Mean Climate

R. J. STOUFFER,[a] J. L. RUSSELL,[a] R. L. BEADLING,[a,b,c] A. J. BROCCOLI,[d] J. P. KRASTING,[e] S. MALYSHEV,[e] AND Z. NAIMAN[f]

[a] *Department of Geosciences, The University of Arizona, Tucson, Arizona*
[b] *University Corporation for Atmospheric Research, Boulder, Colorado*
[c] *Atmospheric and Oceanic Sciences Program, Princeton University, Princeton, New Jersey*
[d] *Department of Environmental Sciences and Institute for Earth, Ocean, and Atmospheric Sciences, Rutgers, The State University of New Jersey, New Brunswick, New Jersey*
[e] *Geophysical Fluid Dynamics Laboratory, NOAA, Princeton, New Jersey*
[f] *TuSimple, Inc., Tucson, Arizona*

(Manuscript received 2 September 2020, in final form 13 November 2021)

ABSTRACT: Climate models of varying complexity have been used for decades to investigate the impact of mountains on the atmosphere and surface climate. Here, the impact of removing the continental topography on the present-day ocean climate is investigated using three different climate models spanning multiple generations. An idealized study is performed where all present-day land surface topography is removed and the equilibrium change in the oceanic mean state with and without the mountains is studied. When the mountains are removed, changes found in all three models include a weakening of the Atlantic meridional overturning circulation and associated SST cooling in the subpolar North Atlantic. The SSTs also warm in all the models in the western North Pacific Ocean associated with a northward shift of the atmospheric jet and the Kuroshio. In the ocean interior, the magnitude of the temperature and salinity response to removing the mountains is relatively small and the sign and magnitude of the changes generally vary among the models. These different interior ocean responses are likely related to differences in the mean state of the control integrations due to differences in resolution and associated subgrid-scale mixing parameterizations. Compared to the results from $4xCO_2$ simulations, the interior ocean temperature changes caused by mountain removal are relatively small; however, the oceanic circulation response and Northern Hemisphere near-surface temperature changes are of a similar magnitude to the response to such radiative forcing changes.

KEYWORDS: Ocean; Ocean circulation; Paleoclimate

1. Introduction

Climate models have been used to study the impact of mountains on Earth's climate for almost 50 years. Some of these studies have used realistic or idealized past topography (e.g., Barron and Washington 1984; Feng and Poulsen 2014; Maroon et al. 2015; Singh et al. 2016). Other idealized studies have been performed where topography is removed or lowered globally (e.g., Manabe and Terpstra 1974; Kutzbach and Guetter 1989; Kutzbach et al. 1993; Manabe and Broccoli 1990; Broccoli and Manabe 1992; Kitoh 1997, 2004; Abe et al. 2004; Takahashi and Battisti 2007a,b; Kitoh 2007; Schmittner et al. 2011; Sinha et al. 2012) or added or removed selectively (e.g., Xu et al. 2004; Boos and Kuang 2010, 2013; Maroon et al. 2015; Baldwin et al. 2019; Lutsko et al. 2019). All of these studies have focused on the atmospheric response to the changed topography.

Here we focus on how the removal of all of Earth's continental topography impacts the present-day oceanic mean state using three different coupled climate models. The results from the experiments highlight the impact that mountains exert on the oceanic mean state through changes in the surface wind stress field and buoyancy flux. Two of the models, ESM2Mb and ESM2G, are Earth system models (ESMs) developed by the Geophysical Fluid Dynamics Laboratory (GFDL) of the National Oceanic and Atmospheric Administration (NOAA) (Dunne et al. 2012, 2013). ESM2Mb and ESM2G use common atmospheric, land surface, and sea ice components, differing only in their oceanic components. The third model, the Manabe Climate Model (herein MCM-UA) is an atmosphere–ocean general circulation model (AOGCM), developed at GFDL and used extensively in the 1990s. All MCM-UA simulations for this study were performed at the University of Arizona (UA). With much simpler physical parameterizations and a coarser grid, the MCM-UA is approximately 300 times less expensive to integrate compared to the ESMs.

Analogous to the earlier studies in which the influence of the mountains on the atmosphere were investigated, this study seeks to understand the role that continental topography plays in the ocean's climate. The expectation prior to conducting the analysis was that the oceanic response to removing the mountains would be similar among the three models. This assumption was based on two lines of reasoning. First, surface forcing changes are fairly similar among the models (shown below), suggesting that the oceanic responses would also be similar. Second, Krasting et al. (2018) found, using integrations that were in a near-statistical equilibrium state with preindustrial and increased atmospheric CO_2

Corresponding author: Ronald J. Stouffer, ronaldstouffer@arizona.edu

DOI: 10.1175/JCLI-D-20-0690.1

concentrations, that both the transient and equilibrium atmospheric and oceanic responses were remarkably similar in the two ESMs used here (ESM2Mb and ESM2G). The MCM-UA model also produces similar transient and equilibrium changes relative to the ESMs when forced with increased atmospheric CO_2. These two lines of reasoning suggest that similar large-scale oceanic responses should occur when the mountains are removed.

Previous work found that removing topography results in primarily three large-scale changes to Earth's climate: 1) midlatitude westerly winds become more zonal (e.g., Manabe and Terpstra 1974), 2) the Asian monsoon circulation weakens (e.g., Kitoh 2004; Lee et al. 2015), and 3) global surface temperatures rise by 1°–1.5°C (Barron 1985; Kutzbach et al. 1993; Kitoh 1997). Using the same ESMs used here (ESM2Mb and ESM2G), Naiman et al. (2017) found similar atmospheric responses to mountain removal to the previous studies cited above; however, the authors also found large changes in the Walker circulation, attributed to large changes in El Niño–Southern Oscillation (ENSO) in the two models. These atmospheric circulation changes caused part of the rainfall maximum currently located over and near the Maritime Continent to migrate toward eastern Africa.

In the remainder of this paper, we will focus on the responses of the ocean to the removal of the land topography in the three models. The outline of the paper is as follows: A brief model description and experimental design is given in section 2, and the results of the experiments where the mountains are removed and the experiments where CO_2 increased are presented in section 3. A discussion of the reasons for our original hypothesis being incorrect is given in section 4. A brief summary is given in section 5.

2. Model description and experimental design

a. GFDL Earth system models

The two GFDL ESMs, ESM2Mb and ESM2G, have identical atmosphere, ice, and land surface components (Dunne et al. 2012, 2013) and differ only in their oceanic components. ESM2Mb uses the Modular Ocean Model version 4.1 (MOM4.1), with a depth-based vertical coordinate, and is very closely related to ESM2M documented in Dunne et al. (2012, 2013) with the only difference being the adoption of vegetation parameters to be more consistent with ESM2G and observations of global biomass. ESM2G uses the Generalized Ocean Layer Dynamics ocean component (GOLD; Hallberg 1995; Dunne et al. 2012) with an isopycnal vertical coordinate. For the integrations described here, the atmospheric CO_2 concentration in the ESMs is kept at a constant value of 286 ppm. Both models resolve the diurnal cycle using a 3-h radiation time step and use a 30-min time step for solving the atmospheric dynamics. A 1-h time step is used for oceanic variables and coupling between model components (Dunne et al. 2012, 2013). Both models use an atmospheric grid with 2.5° longitude × 2° latitude spacing and a 1° longitude × 1° latitude grid spacing (telescoping to 1/3° latitude spacing near the equator) in the oceanic component.

A 1000-model-year spinup period occurred in both models before year 1 of the CONTROL integration was declared. The no mountain integration, NOMTN, was initiated from 1 January, year 1 of the CONTROL. Given this relatively short spinup time period, it is likely that neither model is in a near-equilibrium state at the start of the CONTROL integrations as discussed below. For this study, the length of the ESM2Mb CONTROL and NOMTN integrations are 1500 and 500 years, respectively. For ESM2G, the CONTROL integration is 1000 years in length and the NOMTN integration is 1500 years (Fig. 1). The time mean physical climate and response to changes in forcing due to greenhouse gases (GHGs) are very similar between ESM2G and ESM2Mb (Krasting et al. 2018).

To assess the relative magnitude of the oceanic response to mountain removal, we contrast the NOMTN results with 4 times preindustrial CO_2 integrations ($4xCO_2$) in which atmospheric CO_2 concentrations are instantaneously quadrupled from a CONTROL state. The $4xCO_2$ ESM integrations are in a near-equilibrium state (Krasting et al. 2018). The CONTROL integrations for the $4xCO_2$ integrations are a continuation of the same CONTROL integrations used for the NOMTN experiments. The increased CO_2 integrations branched off the CONTROL at model year 1, which (as noted above) is after 1000 model years of spinup. The $4xCO_2$ integrations are 5000 years in length and the last 100-yr time averages are used here.

b. MCM-UA AOGCM

The Manabe Climate Model (MCM) is fully described in Delworth et al. (2002) and references therein. A short summary description is given at http://u.arizona.edu/~ronaldstouffer/MCM_Description_Summary.html. The model was developed in the 1980s and 1990s by S. Manabe and collaborators at NOAA's GFDL. A lower-resolution model version was first developed in the mid-1980s and used a 4.5° latitude × 7.5° longitude grid spacing in the atmospheric component. The higher-resolution model presented here has a 2.25° latitude × 3.75° longitude (~250 km) horizontal resolution in the atmosphere, which is slightly coarser than, but roughly comparable to, many of the climate and ESMs used in phase 5 of the Coupled Model Intercomparison Project (CMIP5; see Table 6.11 in Ciais et al. 2013). While the grid spacing is similar to CMIP5 models, particularly in the oceanic component, most of the physical subgrid-scale parameterizations in all components are simplified. This enables the model to be very inexpensive in terms of present-day computer resources, allowing many climate studies to be performed economically. The MCM-UA model occupies a place in the hierarchy of climate models that lies between Earth system models of intermediate complexity (EMICs) and modern AOGCMs. It has a more complete representation of atmospheric and oceanic dynamics than most EMICs, but simpler physical parameterizations than current CMIP-class AOGCMs. Despite its simplicity relative to other climate models and ESMs currently in use, MCM-UA has been shown to perform very well relative to other more sophisticated and

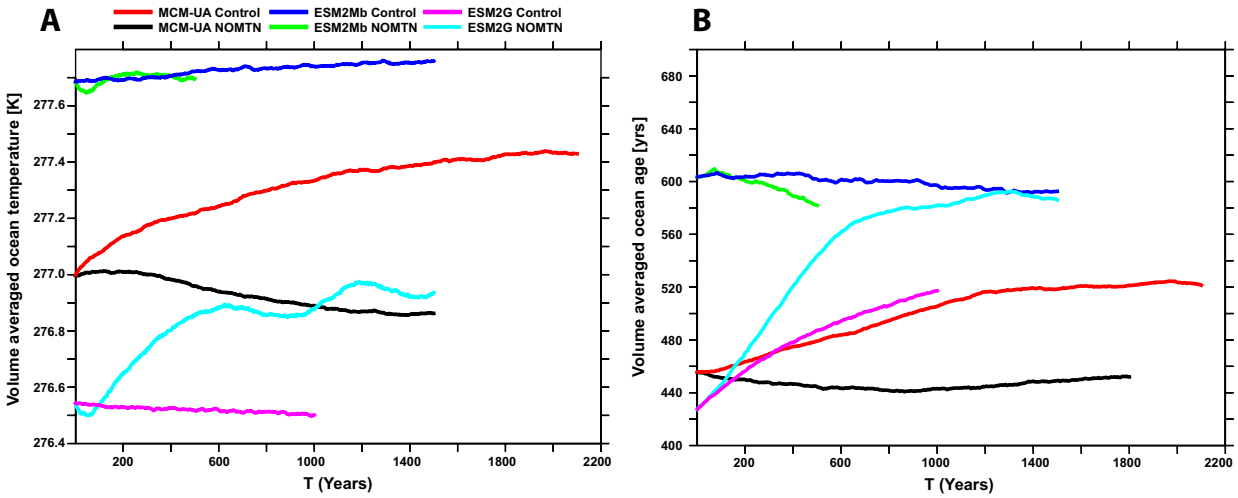

FIG. 1. Time series of CONTROL and NOMTN globally and volume averaged (a) ocean temperature (K) and (b) ideal age tracer (years since surface contact) from the three models. Note that there is a spinup period before year 0 of the CONTROL that is not shown; in the ESMs, the spinup period is 1000 years and in MCM-UA, this period is 2100 years.

state-of-the-science CMIP6 models in climatically important regions such as the Southern Ocean (Beadling et al. 2020).

The oceanic component is a slightly modified version of the MOM1 ocean model (Pacanowski et al. 1991). The horizontal grid is 192 grid locations east–west and 80 north–south, amounting to a nominal horizontal resolution of ~2.25° latitudinally. The vertical grid uses 18 levels at fixed depths, with finer vertical grid spacing near the surface, and a 40-m-deep surface layer grid box. The atmosphere component uses a spectral method to solve the equations of motion. The truncation used is rhomboidal at 30 waves retained (R30). These waves are resolved on a grid that uses 96 east–west grid locations by 80 north–south. The atmospheric component uses 14 vertical sigma levels.

Coupling between the atmosphere–ocean/sea ice is performed once per day. Radiation is computed once per day; no diurnal variations are simulated by the model. The heat, freshwater fluxes, and wind stress are passed to the ocean once per day. The coupling is serial, where the atmosphere runs one day and then the ocean integrates that same day using the atmospheric fluxes and providing the sea surface temperature (SST) and sea ice to the atmosphere for its lower boundary at the start of the next day. Both heat and freshwater flux adjustments (Manabe and Stouffer 1988) are used to minimize climate drift in the control integration, while maintaining realistic SST and SSS distributions. These adjustments are a function of grid location and month of the year, but they have no variations on time scales longer than one year. The adjustments are computed prior to the start of the control integration and are exactly the same for all perturbation integrations. As shown in Manabe and Stouffer (1988) and Manabe et al. (1991), the use of these adjustments reduces model surface drift and maintains realistic SST and SSS fields.

The CONTROL integration was initiated in the 1990s at GFDL on a CRAY machine. The model and restart data for model year 2100 (model started at model year 1) was ported to the High Performance Computing (HPC) system at the University of Arizona in 2017 and the model was renamed the Manabe Climate Model–University of Arizona (MCM-UA). The NOMTN integration was started from 1 January 2101 of the CONTROL. For the discussion here, the CONTROL integration prior to the port is considered spinup. As a result, 1 January 2101 is year 1 in all MCM-UA plots and figures presented here. Finally, we note that the computational cost of MCM-UA is minimal on the UA HPC, although storage costs are not negligible.

As mentioned above, the results of the NOMTN simulations are compared to a $4xCO_2$ integration. The MCM-UA $4xCO_2$ integration is also in a near-equilibrium state. The $4xCO_2$ integration branched off the CONTROL at model year 1 just after the spinup period. The increased CO_2 integration is 5600 years in length and the last 100-yr time averages are used here.

c. *Experimental design*

Simulations with the ESMs and MCM-UA were conducted with present-day topography (CONTROL) and all topography removed (NOMTN). To avoid transient or time-dependent influences on the response to removing the mountains, all of the models were integrated toward a nearly statistical steady state (i.e., variability is still present in the simulation, but the mean climate does not change) meaning the long-term volume-averaged ocean temperature is stable and the top of atmosphere net radiation is near zero. It takes several thousand model years to reach such a steady state, making such integrations with the ESMs computationally expensive.

In all NOMTN simulations, the river routings and the geographic distribution of albedo associated with high-latitude ice sheets (i.e., Antarctica and Greenland) were not changed. The prescribed ice sheets remain white in the NOMTN as in the CONTROL simulations, assuming an ice-sheet-covered

surface. However, the topography associated with the ice sheets is set to 0 m. The ocean bathymetry, surface roughness, and sea level are not changed between the CONTROL and NOMTN integrations. Consistent with flattening of the model topography, the topographic momentum drag scaling scheme in all the models and the gravity wave drag scheme in the ESMs were turned off in the NOMTN integrations. MCM-UA only incorporates a gravity wave drag scheme, which was turned off in the NOMTN integration. The CONTROL and NOMTN experiments are integrated with preindustrial radiative forcing (~286 ppm).

As discussed below, there is climate drift evident in the ESM CONTROL simulations, even at the end of the integrations. The last 100 years of the ESM2Mb and ESM2G CONTROL and NOMTN integrations are used here unless otherwise noted. As mentioned above, the MCM-UA integrations (CONTROL and NOMTN) are time integrated for 2200 model years after the spinup period and are very near an equilibrium state as discussed below. For much of the analysis presented here, the last 300 years of the MCM-UA CONTROL and NOMTN integrations are used. Since MCM-UA is near equilibrium, a longer time averaging period can be used to reduce the influence of variability on the results presented here.

3. Results

a. *Approach to equilibrium*

Before evaluating the oceanic response to removing the mountains, we diagnose the degree to which the integrations in the three models are equilibrated. This is followed by a brief assessment of the ocean properties in each model's CONTROL simulation relative to observations and to each other.

Near the end of their respective CONTROL and NOMTN integrations, all models show minimal trends in volume averaged ocean temperature (Fig. 1a). The ESMs show slightly larger trends in their CONTROL integrations compared to MCM-UA. Long time scale variability is found in the ESM NOMTN integrations. The sources of this variability have not been investigated in detail, although Krasting et al. (2018) show changes in the Atlantic meridional ocean circulation (AMOC) and gyre circulations on 1000-yr time scales that may contribute to these temporal patterns.

The volume-averaged ocean temperature in ESM2Mb exhibits little change (~0.1°C) between the CONTROL and NOMTN integrations (Fig. 1a), although the NOMTN integration is short (500 years) relative to the ESM2G and MCM-UA NOMTN integrations. Unfortunately, changes to computing systems at GFDL since the ESM2Mb NOMTN simulation was performed prevent the extension of this experiment. In ESM2G, the ocean warms when the mountains are removed, while in MCM-UA the ocean cools as the climate approaches an equilibrium. These changes in volume averaged ocean temperature in response to the mountain removal are relatively small compared (≤0.5°C) to changes that occur in response to other climate perturbations such as large increases in atmospheric CO_2. To put this in perspective, at equilibrium, the volume averaged ocean temperature in ESM2Mb and ESM2G warms by more than 4°C in a 4xCO_2 simulation (implying roughly a 2°C warming for doubling; Krasting et al. 2018). This is discussed in section 3e of this paper.

Another way to evaluate the approach to equilibrium is through an idealized age tracer (Fig. 1b). The values are in units of time (years) since the water has been at the ocean surface (Thiele and Sarmiento 1990). The MCM-UA CONTROL and NOMTN integrations are very near a steady state or equilibrium by the end of the integrations. However, the ESM2Mb and ESM2G NOMTN integrations show clear trends in ocean age, with a decrease in ESM2Mb (implying increased ocean ventilation) and an increase in age in ESM2G (implying reduced ocean ventilation). The ESM2G NOMTN integration appears to be close to approaching an equilibrium state, although a longer integration is required for confidence in that assessment.

Taken together, the ocean volume averaged temperature and age time series suggest that the MCM-UA integrations presented here are close to equilibrium, while the ESM integrations are both in a transient state. The ESM2G integrations may be closer to a steady state than ESM2Mb if our assessment of the ESM2G NOMTN integration is correct. Given that among the three models, only the MCM-UA results are in a near-equilibrium state and given the relative quality of its simulation (as discussed below), we include it in this study.

b. *Assessment of CONTROL ocean state across models*

Here we compare the CONTROL integration to the near present-day observations of temperature and salinity, using the *World Ocean Atlas 2013* (*WOA13*) product (Boyer et al. 2013; Figs. 2 and 3, left panels) as the observational benchmark. Given that observations indicate that the ocean has warmed over the past few decades, we do not expect the modeled ocean state to exactly match that observed since the preindustrial control integrations do not contain the anthropogenic warming signal (Gebbie and Huybers 2019; Zanna et al. 2019). While the exact amount and distribution of ocean warming since the preindustrial period is not known, model results suggest that the anthropogenic signal is largest near the surface and rapidly decreases with increasing depth (e.g., Manabe et al. 1991; Cubasch et al. 2001). In the high latitudes where this generalization is less true, the warming at depth is likely to be smaller than 0.1 K (the contour interval in Fig. 2; Collins et al. 2013). Thus, we should expect to find the upper ocean slightly cooler than the *WOA13* product in the CONTROL integrations, all other things being equal. While we do not expect the models to agree with the observed for the reasons discussed above, we use this assessment to identify large errors that may distort the oceanic response to removing the mountains.

In the Atlantic Ocean, the difference patterns in all three models (CONTROL minus *WOA13*) look generally similar with the upper 1000 m in the tropical and subtropical oceans

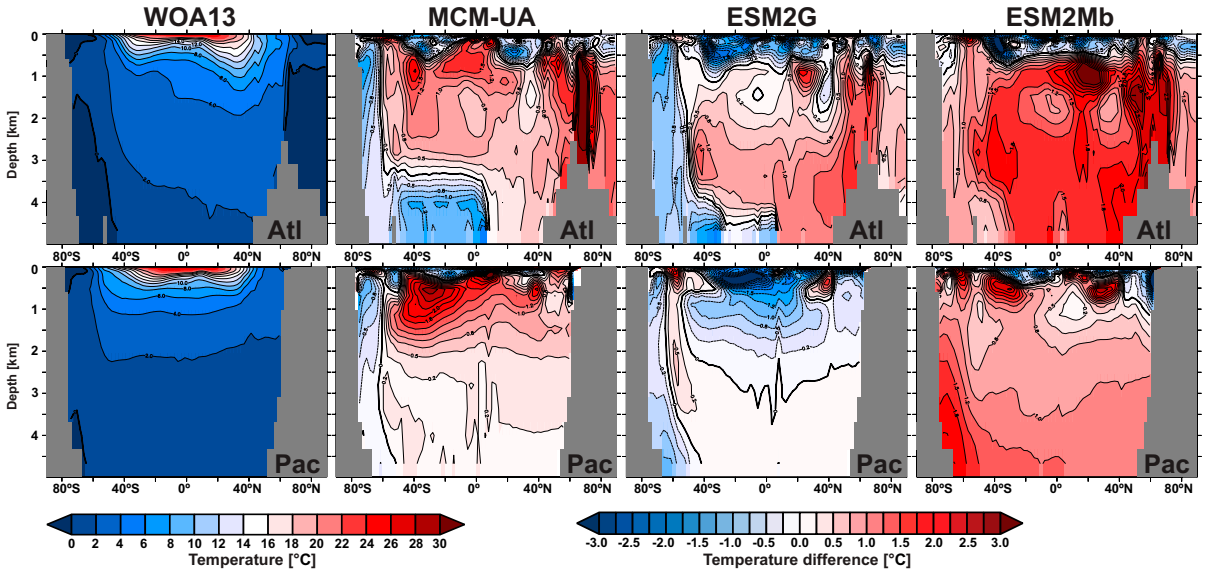

FIG. 2. Zonally averaged ocean temperature and difference (°C) computed as CONTROL minus observed, for (top) Atlantic only and (bottom) Pacific only. Observational values are from the *World Ocean Atlas 13* (*WOA13*) product averaged over all available observations (Boyer et al. 2013). The observations and model results are interpolated onto a common 2° grid. The bathymetry (gray shading) on this and all latitude–depth figures that follow is for latitudes that are land at all grid locations in the zonal belt.

being relatively cold compared to *WOA13*, as expected due to the lack of the anthropogenic warming signal (Fig. 2). MCM-UA is slightly different in that it shows warmer than observed temperatures in the tropics. In each model, these relatively colder regions in the upper ocean overlie anomalously warmer (relative to *WOA13*) water at depth extending from the Arctic to the midlatitude Southern Ocean. The models differ mainly in their temperature structure in the Southern Ocean near the Antarctic continent. Near Antarctica in both MCM-UA and ESM2G, there is a region of too cold waters that extends throughout the water column from the surface to the abyssal ocean and northward at the ocean bottom toward the equator. In ESM2Mb there is also a small cooling region in the upper few hundred meters near Antarctica. However,

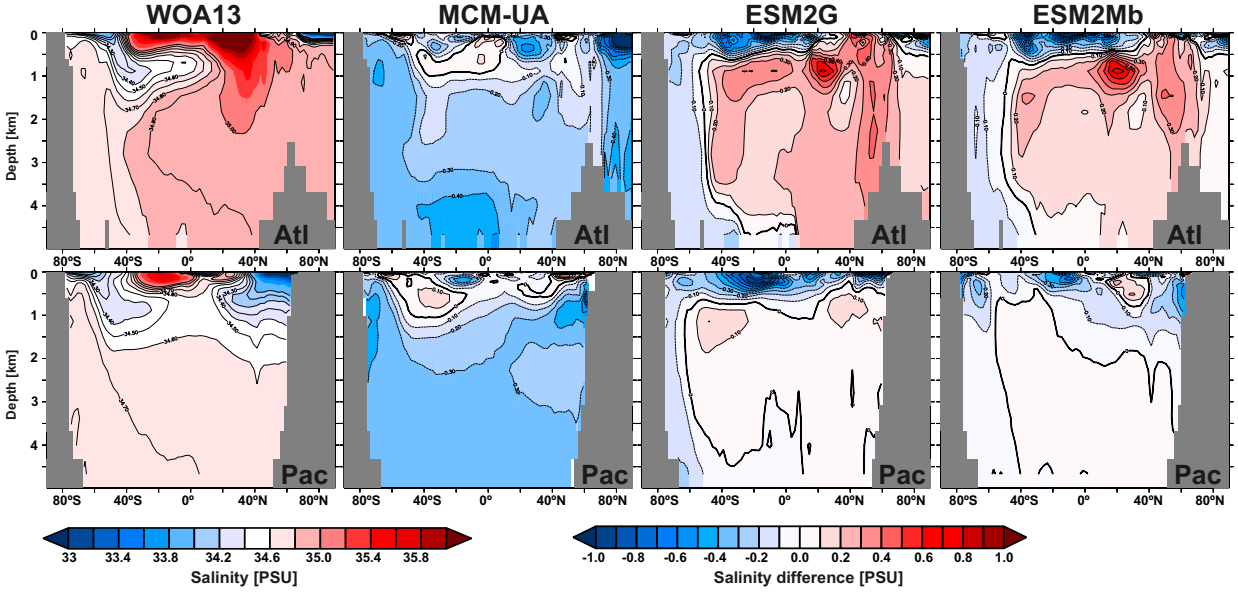

FIG. 3. Zonally averaged ocean salinity and difference computed as CONTROL minus observed, for (top) Atlantic only and (bottom) Pacific only. Observational values are from the *WOA13* product (Boyer et al. 2013). The observations and model results are interpolated onto a common 2° grid.

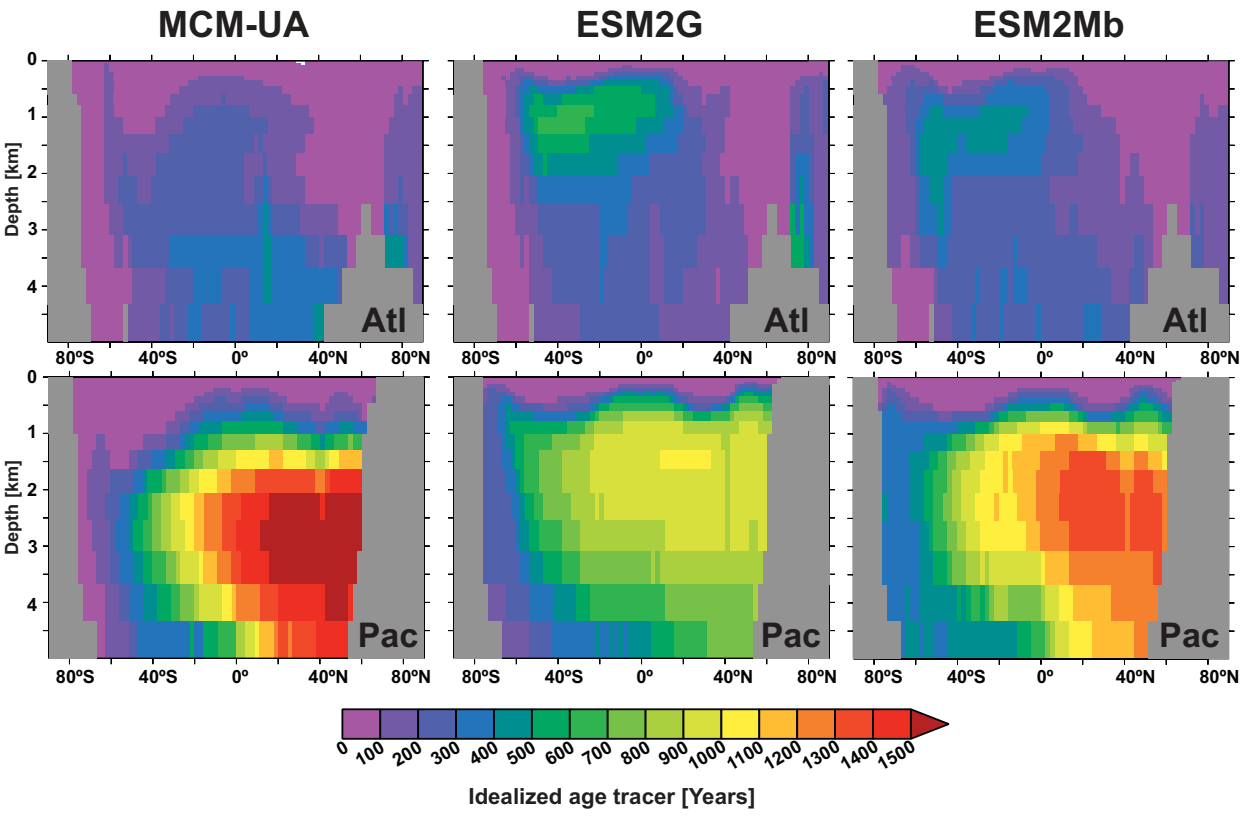

FIG. 4. Zonally averaged idealized age tracer (years since the water was last at the ocean surface) taken from CONTROL integrations averaged only over the (top) Atlantic Ocean and (bottom) Pacific Ocean. The model results are interpolated onto a common 2° grid.

the rest of the global ocean below this depth (including near the Antarctic continent) is too warm relative to that observed. The magnitude of this warm bias at depth is also much larger than in the other two models. Given that there is a warming trend in ESM2Mb (Fig. 1), this warm bias should continue to grow as the model nears equilibrium.

In the Pacific Ocean, the error patterns look similar to the Atlantic patterns discussed above in MCM-UA and ESM2Mb (Fig. 2). In ESM2G, the temperatures below ~2 km are close to the observed values. Put together, one can see that ESM2Mb has the warmest ocean volume averaged temperature as shown in Fig. 1a, and ESM2G is the coldest of the three models and closest to that observed. The MCM-UA ocean temperature differences from observations below 2 km and ocean volume temperature biases lie between the two ESMs.

Considering salinity, the MCM-UA is fresher than *WOA13* at most latitudes and depths in both the Atlantic and Pacific Oceans (Fig. 3). In both the ESMs, there is a tendency to be too fresh near the surface and throughout the ocean near Antarctica (Fig. 3). Both ESM2G and ESM2Mb are too saline compared to *WOA13* in the Atlantic below ~500 m. However, this enhanced salinity in ESM2Mb and ESM2G below ~1 km is smaller in magnitude in the Pacific Ocean.

To begin to assess how the different mean-state temperature and salinity structures impact ocean vertical mixing and circulation, we diagnose the structure of the ideal age tracer in each model (Fig. 4). The Atlantic is much younger than the Pacific away from Antarctica in all three models (Fig. 4). In the Atlantic, the ages and pattern are similar among the models with the exception of the waters above ~2 km in the Southern Ocean and extending toward the equator. Here the MCM-UA waters are much younger than the corresponding waters in the ESMs. It is likely that this is an error in the MCM-UA simulation associated with excessive open ocean convection in the Southern Ocean adversely impacting the intermediate water properties formed in this region and potentially the response to removing the mountains. However, as noted by Dunne et al. (2012), ESM2G's intermediate waters are underventilated in the South Atlantic, resulting in older than expected waters.

In the observed ocean, the oldest waters are found in the Pacific Ocean near 2-km depth at ~40°N with an age of approximately 1000 years (Matsumoto 2007). The ESM2G ideal ages are very close to the observed estimate. The MCM-UA waters are nearly 500 years older than the corresponding waters in ESM2G, suggesting weaker ventilation of the deep ocean. In ESM2Mb, these waters are about halfway in terms of age between the other two models. The ESM2Mb and

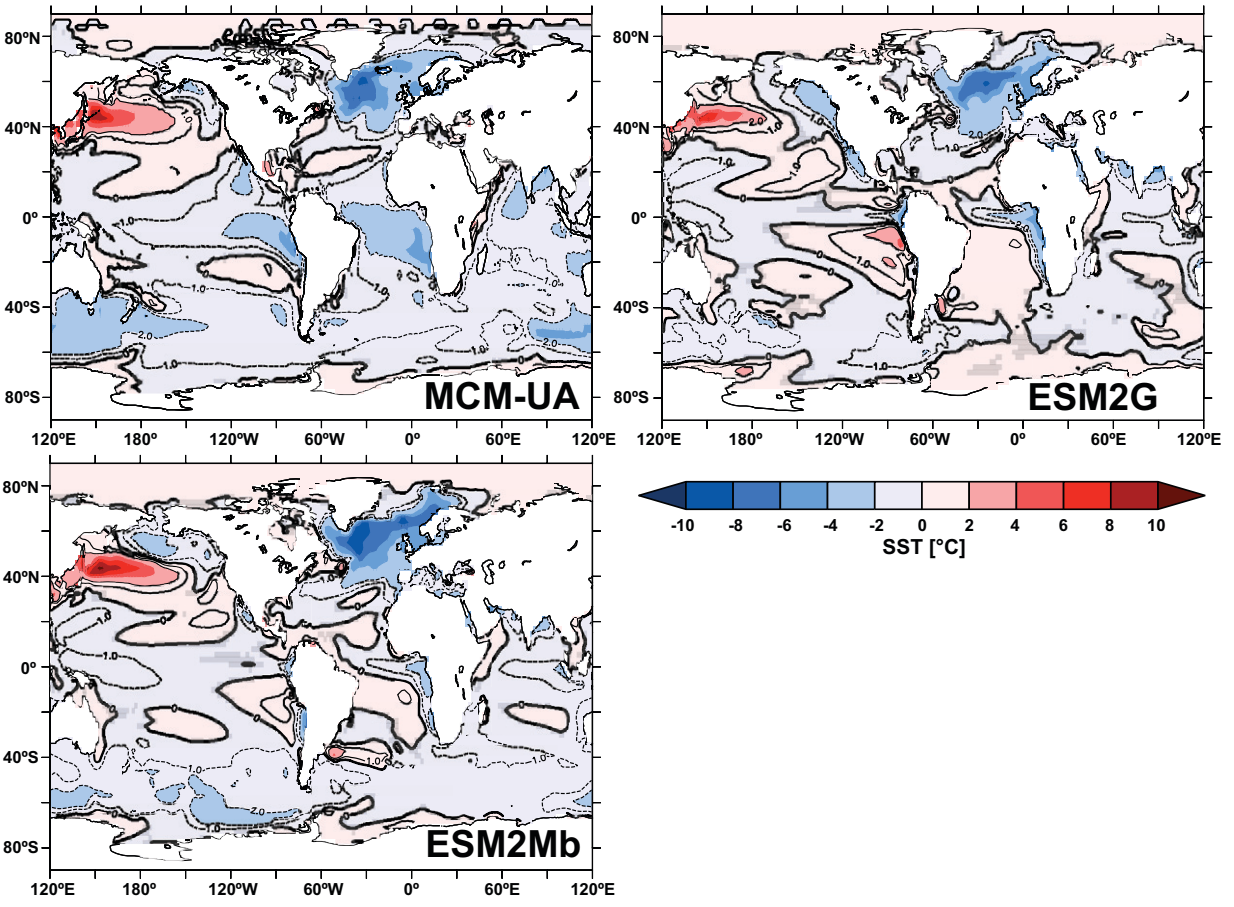

FIG. 5. Sea surface temperature (SST; °C) difference NOMTN minus CONTROL. ESM2G and ESM2Mb data are interpolated into the MCM grid to aid in the comparison. The MCM-UA values are a 300-yr time average obtained from the end on the integrations presented in Fig. 1. ESM2Mb values are a 100-yr time average from model years 401–500. ESM2G values are a 100-yr time average from model years 901–1000. These time periods are used for all the following figures unless otherwise noted. Contours range from −2° to 2°C with a 1° interval. Gray shading indicates grid points that fail a two-tailed Student's *t* test for the difference being statically significant at the 95% confidence level. The number of independent years is assumed to be 60 for the ESMs and 200 for MCM-UA. Here we assume that the number of independent samples is 2/3 the total length of the annual time series. Boer (2000) found that for annually averaged SST, there is little correlation of anomalies from one year to the next outside of the tropical Pacific (ENSO region), the Southern Ocean, and the northern North Atlantic. This suggests that using 2/3 of the time series length is a valid assumption for SST in most regions. The time periods chosen for computing the test are the same periods chosen for the averaging.

ESM2G results shown here are very similar to those found in Fig. 13 of Dunne et al. (2012) and the readers are encouraged to see Dunne et al. (2013) for an in-depth discussion of the differences of the ideal age tracer distributions between the two ESMs. The sluggish ventilation of the deep ocean in MCM-UA and ESM2Mb may impact the response of the model to removing the mountains. Also, it shows that ESM2Mb is likely in a transient state and not at equilibrium due to the shortness of the NOMTN integration (500 years), since the oldest water in the Pacific in the CONTROL integration is older than the length of the NOMTN integration. ESM2G also is likely not near equilibrium in its CONTROL (1000 years). As discussed above, the ESM2G NOMTN (1500 years) integrations may be near an equilibrium state. The MCM-UA with its very long spinup (2100 years) prior to the start of the experiments shown here is likely the only model used here in a near equilibrium state by the end of its integrations.

c. *Surface response to removing the mountains*

1) SEA SURFACE TEMPERATURE RESPONSE

The changes in near-surface temperature that occur when the mountains are removed are examined using maps of the sea surface temperature (SST) difference (NOMTN minus CONTROL; Fig. 5). SST is shown instead of surface air temperature (SAT) because SAT difference plots are dominated by warming anomalies where the mountains are removed attributed to the decrease of atmospheric temperature with height.

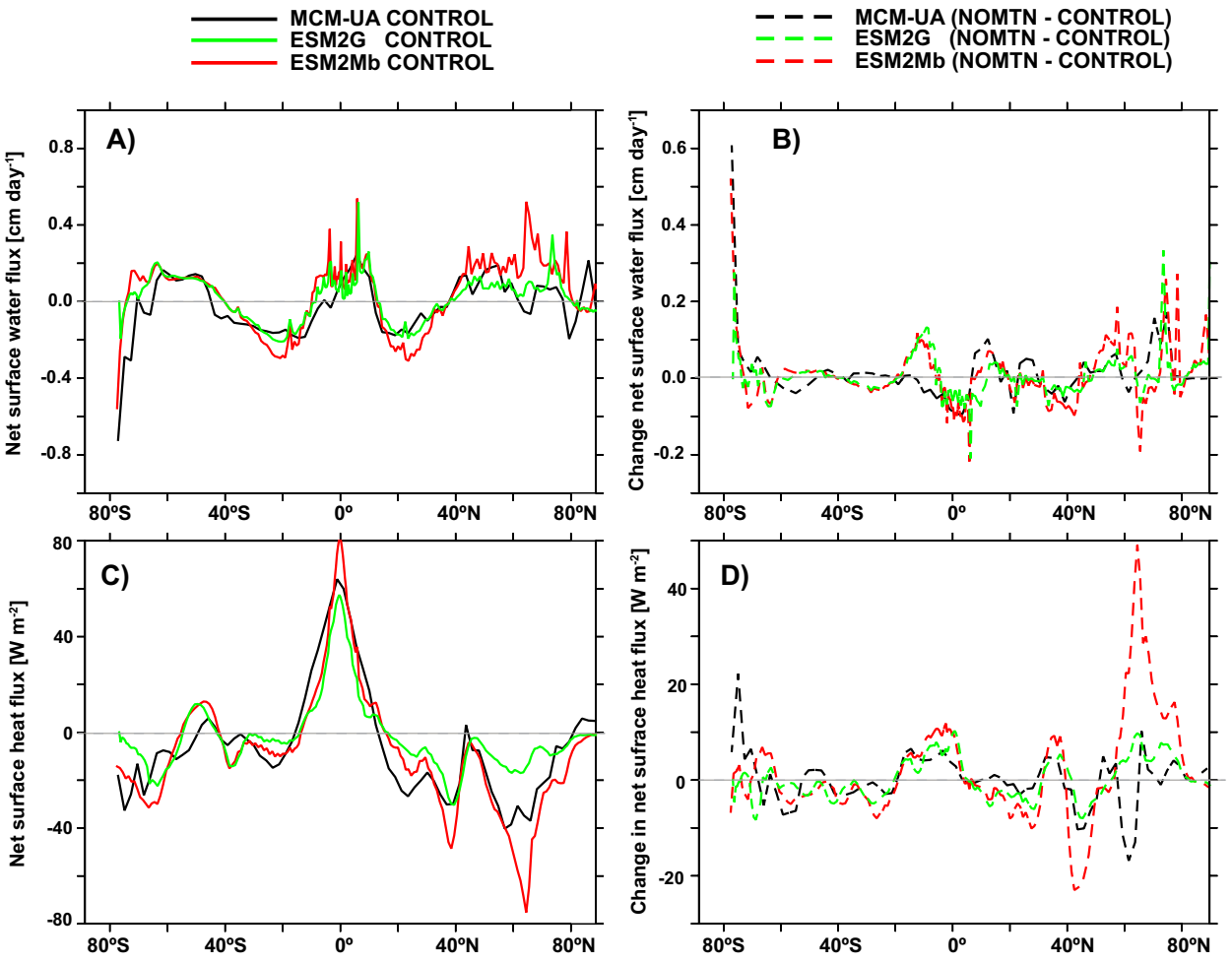

FIG. 6. Zonally averaged (over the ocean only) surface fluxes: (a) CONTROL net surface water flux into the ocean (precipitation − evaporation + runoff including sea ice effects; cm day^{-1}), (b) NOMTN − CONTROL net surface water flux into the ocean (precipitation − evaporation + runoff including sea ice effects; cm day^{-1}), (c) CONTROL net surface heat flux into the ocean (positive values tend to warm the ocean; W m^{-2}), and (d) NOMTN − CONTROL net surface heat flux into the ocean (positive values tend to warm the ocean; W m^{-2}). Time periods are the same as those in Fig. 5.

Several robust spatial patterns emerge across the three models in the SST anomalies when the mountains are removed. All models exhibit a cooling of about 6°C in the high-latitude North Atlantic. This cooling is largest in ESM2Mb relative to the other two models, and is likely linked to the larger change in the AMOC in ESM2Mb as discussed below. There is a region to the southwest of the large cold anomalies off the east coast of North America where surface warming is found from the Cape Hatteras region (~40°N) to the mouth of the St. Lawrence River in all three models. In the western North Pacific, there is a 4°–6°C warming over the Kuroshio Extension region likely related to the northward shift of the atmospheric jet and expansion of the subtropical gyre northward as discussed below. All models also show cooling at the surface in most eastern boundary upwelling regions.

There are some notable regional differences between the models. In ESM2Mb and MCM-UA, there is a small region of cooling in the southern South Pacific Ocean, while the sign changes are mixed in ESM2G in the same region. Takahashi and Battisti (2007a) found a warming in the SSTs in the tropical/subtropical region west of the Andes when the Andes are removed. Both ESMs also show a warming in this region while the MCM-UA has a cooling when the mountains are removed. However, one cannot easily say that this differing MCM-UA response is incorrect given the more realistic surface climate in this model, owing to the flux adjustments. In this region in the MCM-UA CONTROL integration, the SSTs are cooler and the low cloud cover is higher relative to the ESMs, as in the observations. The ITCZ is also more realistic in the MCM-UA in that it does not suffer from the "double ITCZ problem" (Lin 2007) nearly to the extent seen in the two ESMs as discussed below.

Despite some regional differences in the response of the models to removing the mountains, the general global pattern

of SST anomalies is similar among the three models. As mentioned previously, the similarity of the SST difference maps across models both in terms of pattern and magnitude is a much more stringent test to evaluate the climate response to removing the mountains than the response of SAT. This is due to the fact that the dominant signal when viewing SAT global maps tends to be that due to lowering the surface elevation to sea level. The fact that the SST response to removing the mountains is also similar among models is notable given the changes highlighted below.

2) Changes in surface buoyancy and momentum fluxes

The zonally averaged net heat flux into the ocean in the CONTROL simulations is similar between the models (Fig. 6a) with oceanic heat gain at low latitudes and heat loss at high latitudes. The largest spread in the zonal averages is found near 65°N where the surface area of the ocean is relatively small and small differences can appear as large changes in the zonal average. The pattern of the annually and zonally averaged net surface water flux also agrees well across the models in their CONTROL simulations, with the largest spread again near 65°N (Fig. 6c). The maximum in net surface water flux found just north of the equator is narrower in MCM-UA as a result of the MCM-UA CONTROL having a single large tropical rain belt north of the equator. The two ESMs' CONTROL integrations have a large rain belt north of the equator with a second slightly smaller rain belt south of the equator. This double rain belt structure is not found in nature (Schneider et al. 2014) yet is a common feature in many coupled climate models and is often referred to as the double-ITCZ problem (Lin 2007).

When the mountains are removed, the changes in the net surface water flux into the ocean are notable in the tropics (Figs. 6a,b). The three models indicate an increase in the water flux into the ocean just north of the equator. Just south of the equator, the ESMs also show a large increase in the net water flux. As noted above, the ESMs have a poor mean-state simulation of the surface water flux in this region, thus these ESM changes in the surface water flux are unreliable. In the middle and high latitudes of the Northern Hemisphere (~40°–60°N), the NOMTN simulations show an increase in the net surface water flux entering the ocean. In the NH, the ESM2Mb maxima and minima are larger than the changes in ESM2G and MCM-UA.

The changes in the net surface heat flux are fairly similar in pattern and magnitude in the three models (Figs. 6c,d). The tropical net surface heat flux maximum shifts toward the south in all three models with the changes tending to warm the ocean just south of the equator. One notable region of large spread in the surface heat flux response between models is northward of ~60°N, where ESM2Mb shows large increases in heat flux into the ocean, ESM2G shows moderate increases, and MCM-UA shows a mixed response. All three models indicate net heat flux changes that would tend to warm the ocean near Antarctica and near 35°N. Again, relatively small oceanic areas in the zonally average may lead to the large difference near Antarctica.

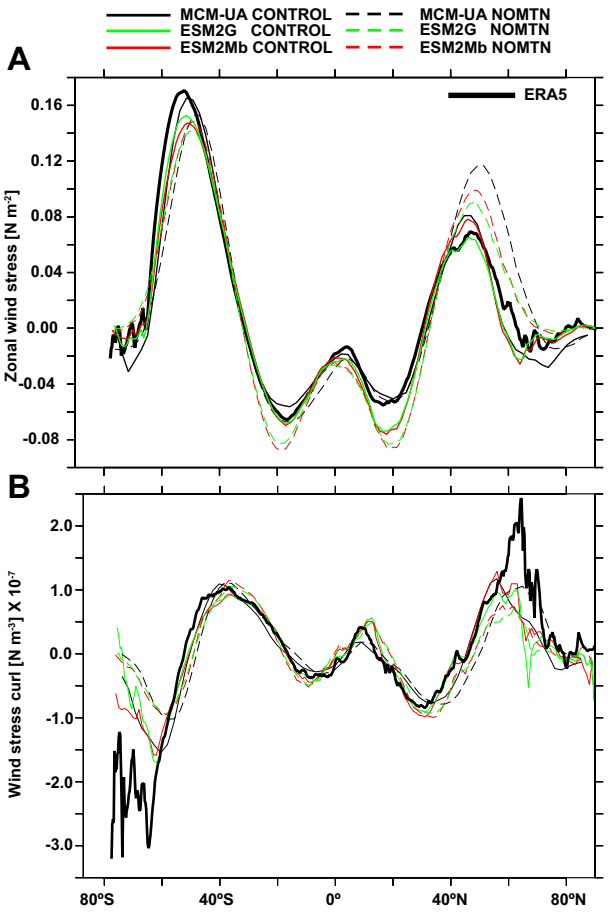

FIG. 7. Zonally averaged (over the ocean only) (a) zonal surface wind stress (positive toward east; N m^{-2}) and (b) wind stress curl [negative (positive) values in the SH (NH) imply upwelling; N m^{-3}] from the CONTROL (solid) and NOMTN (dashed) integrations. Black lines are obtained from the MCM-UA. Red lines are from the ESM2Mb. Green lines are from ESM2G. Time periods are the same as those in Fig. 5. Observations (thick black lines) are from the European Centre for Medium-Range Weather Forecasts (ECMWF) ERA5 atmospheric reanalysis product (https://cds.climate.copernicus.eu/cdsapp#!/dataset/reanalysis-era5-single-levels-monthly-means?tab=overview). Values obtained from the MCM-UA are 300-yr time averages and 100-yr time averages from the ESM2Mb and ESM2G.

The structure and magnitude of the zonally averaged zonal wind stress is similar across models in their CONTROL integrations and consistent with the zonal wind stress pattern from the ERA5 atmospheric reanalysis product (Fig. 7a). Relative to ERA5, both the NH and SH wind stress maximum are located slightly equatorward. As discussed in Beadling et al. (2020), the SH midlatitude jet strength and position in all three models is consistent with other CMIP-class models. The magnitude of the relative minimum located just south of the equator is better simulated in the ESMs while the magnitude of the relative minimum located just north of the equator

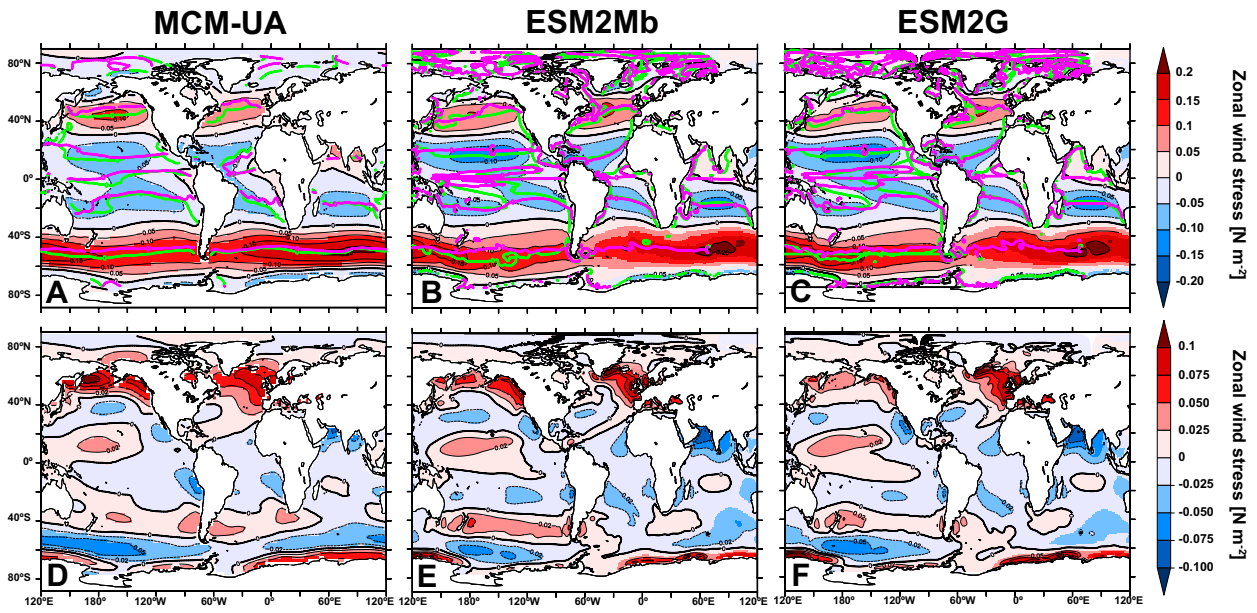

FIG. 8. (a)–(c) Surface wind stress (positive toward the east; N m^{-2}) from the CONTROL integrations and (d)–(f) differences computed as NOMTN minus CONTROL. The zero-wind stress curl contours are also plotted in (a)–(c). Green contours obtained from the CONTROL and purple contours from the NOMTN integrations. Time periods are the same as those in Fig. 5.

is better simulated in MCM-UA. When the mountains are removed, the largest changes are found in middle and high latitudes of the NH as expected given that these latitudes contain many of the world's mountainous regions. Most of the CONTROL maxima and minima shift northward in all the models in the NOMTN integration. The MCM-UA changes near 20°N are relatively small, while the eastward stress shows clear decreases in the ESMs near the minima at 20°S and 20°N. In the SH, the atmospheric SH jet slightly shifts northward and weakens in all three models. The weakening of the SH jet is likely related to the large warming over Antarctica due to the removal of the mountains and ice sheet orography. Warming over the Antarctic continent reduces the meridional temperature gradient, weakening the SH jet. The northward shift in the SH jet is likely due to the NH warming more than the SH when the mountains are removed, shifting the atmospheric circulation northward (Broccoli et al. 2006).

The observed zonally averaged wind stress curl is larger than that found in the three models from 60° to 40°S and near 60°N (Fig. 7b). Outside those regions, the models and observations agree fairly well. The zonally averaged wind stress curl in all three CONTROL integrations is similar in magnitude and location. The maximum positive wind stress curl located just north of the equator is smaller in MCM-UA than in the ESMs. When the mountains are removed, the negative values (indicating Ekman upwelling) in the Southern Ocean are greatly reduced (Fig. 7b). Between 35°S and 35°N, the differences are relatively small but generally shifting the maxima and minima toward the north. North of 35°N, the differences also indicate a shift of the maximum wind stress curl toward the north when the mountains are removed. On the north side of the NH midlatitude jet, the MCM-UA has a much larger and broader shift than the ESMs. Again, these differences are due to the winds becoming more zonal in the NOMTN experiments.

The CONTROL integration wind stress maps look fairly similar among the three models (Figs. 8a–c). The green contours represent the CONTROL integration zero wind stress curl values roughly coinciding with the ocean gyre boundaries. As expected, the zero-wind stress curl contour lies right over the maximum and minimum wind stress values. When the mountains are removed, the NH midlatitude winds become more zonal. In the North Pacific, the winds shift slightly toward the north. This shift can be most easily seen in the shift of the zero-wind stress curl contour in the NOMTN integration [Figs. 8a–c; compare location of green contour (CONTROL) to purple contour (NOMTN)]. The shift is most clearly seen in the MCM_UA plot. This northward shift is also seen in the wind stress difference maps (Figs. 8d–f) near 60°N where the differences indicate much more westerly (or much weaker easterly) winds. In the North Atlantic, the northward shift of the zero-wind stress curl contour is not seen in the ESM results. However, the winds do become more zonally aligned in the North Atlantic as indicated by the relatively large differences near 60°N. The SH midlatitude wind stress maximum shifts northward in the models with the easterly winds weakening along the Antarctic coastline. These changes in the surface wind stress forcing along with changes in the buoyancy forcing in the NH impact the strength of the AMOC as discussed below.

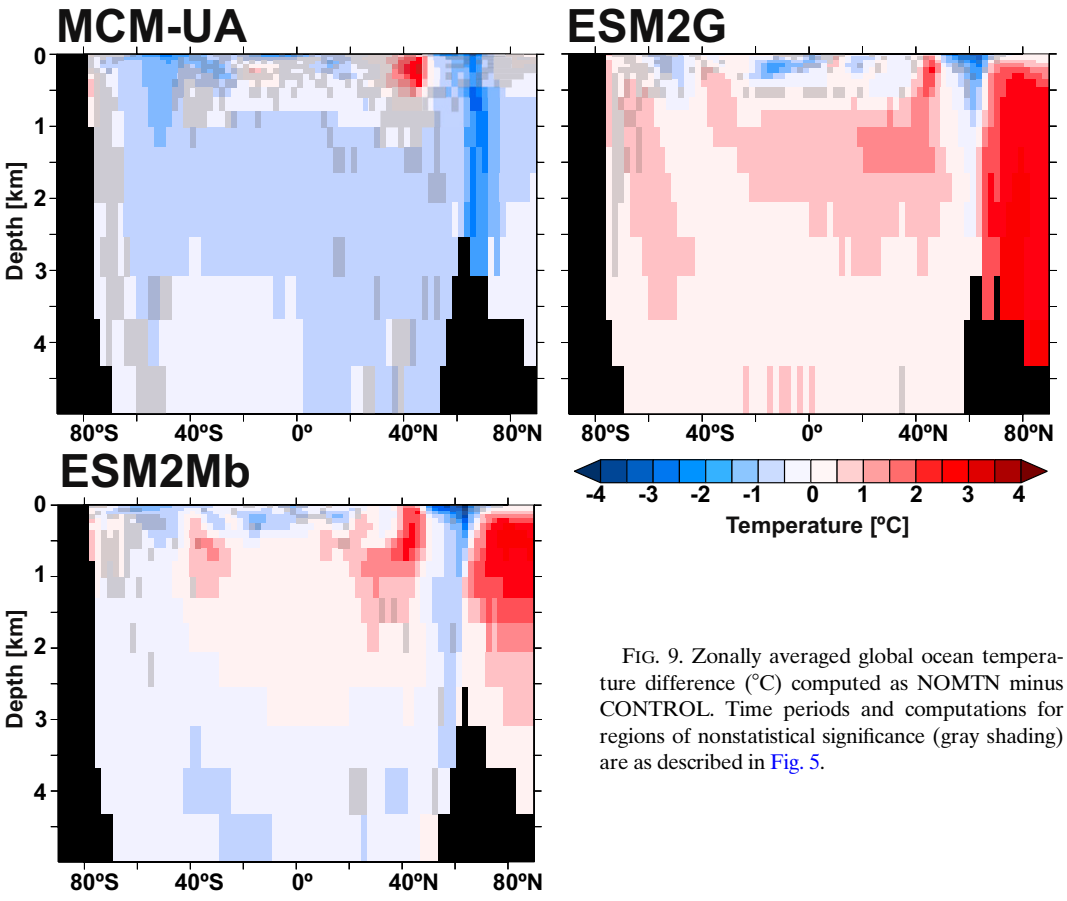

FIG. 9. Zonally averaged global ocean temperature difference (°C) computed as NOMTN minus CONTROL. Time periods and computations for regions of nonstatistical significance (gray shading) are as described in Fig. 5.

d. Subsurface ocean response

Despite similar surface responses, the removal of the mountains results in quite different subsurface ocean anomalies across the models (Fig. 9). In the MCM-UA simulation, there is a general cooling throughout the entire ocean except for a region of warming in the upper 500 m near 40°N. Between 40°S and 40°N there is minimal warming or negligible change between the surface and 1 km. There are small changes in the subsurface temperatures in the Southern Ocean. The largest changes in subsurface temperatures occur in the midlatitude to subpolar NH, with a cooling maximum extending from the surface to 3 km near 65°N, the region of deep-water formation associated with the AMOC.

In ESM2G, there is a general warming throughout the ocean. Similar to MCM-UA, the upper 1 km between 40°S and 40°N shows minimal temperature change (<0.5°C). However, in contrast to MCM-UA, there is a large warming signal below the surface throughout the entire water column in the Arctic Ocean. In ESM2Mb, the subsurface temperature change pattern looks like a mixture of the responses between ESM2G and MCM-UA. In the Arctic above 2 km, the warming is similar in magnitude to ESM2G. Near 40°S, the ESMs show a tongue of subsurface warming extending from the surface to ~1 km in a region dominated by intermediate and mode waters. MCM-UA shows negligible change or slight cooling likely related to the unrealistic vertical mixing in this same region as noted above. The temperature changes in the subpolar Southern Ocean do not agree between the two ESMs, suggesting differing responses in this region to the mountain removal.

As noted above, there are only a few regions where there are similar responses in the three models: 1) a region of minimal change in the upper 1 km between 40°S and 40°N and 2) a region in the vicinity of 65°N, where all the model responses exhibit cooling from the surface to at least 2 km and warming in the upper ocean directly to the south, suggesting a similar AMOC response, which is discussed below.

Similar to subsurface temperature, the subsurface salinity response to removing the mountains differs between the models (Fig. 10). With the exception of the NH subpolar and Arctic regions, large changes in salinity are generally confined to the upper 2000 m in all models. In MCM-UA, the upper 500 m of the ocean in the regions of the subtropical gyres and tropics freshens, which is in contrast to the salinification of these regions in the two ESMs. A region of increased salinity that extends from the surface to ~1500 m is found near 40°N in all three models, however, penetrating deeper in MCM-UA and ESM2G. In MCM-UA a region of increased salinity is found below a few hundred meters in the Southern Ocean

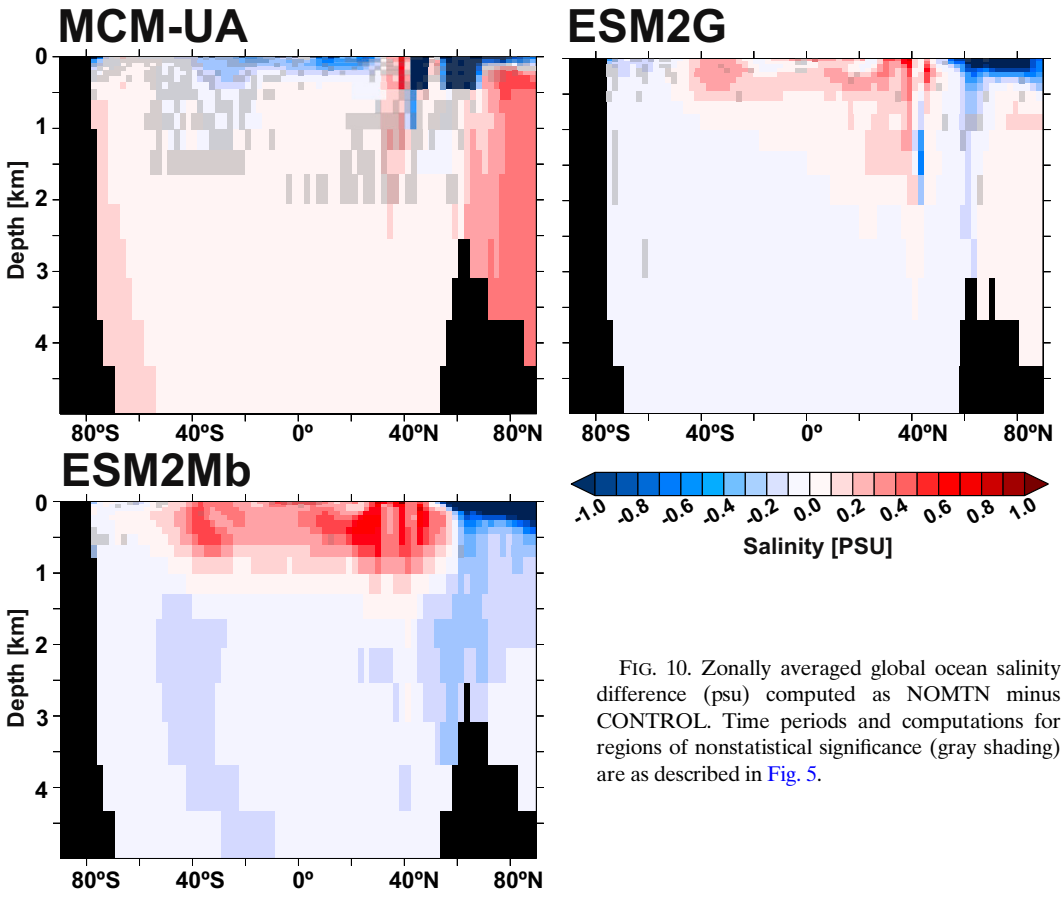

FIG. 10. Zonally averaged global ocean salinity difference (psu) computed as NOMTN minus CONTROL. Time periods and computations for regions of nonstatistical significance (gray shading) are as described in Fig. 5.

south of 60°S and in the Arctic Ocean, with a greater magnitude. With the exception of land-locked inland sea changes near the surface in the NH, most of the changes are small. In ESM2Mb, the salinity response is also generally small, with the exception of the Arctic Ocean above 500 m, where there is a relatively large freshening. This same Arctic freshening is found in ESM2G, but more confined to shallower depths. The salinification of the subtropical gyres in response to removing the mountains is much larger in ESM2G compared to ESM2Mb. Similar to ESM2Mb, ESM2G shows a strong surface freshening in the upper 1 km north of 50°N. The most common feature across models is that minimal salinity changes are found below 1 km.

e. *AMOC response*

The CONTROL Atlantic meridional overturning streamfunction (AMOC) is similar in pattern and magnitude in the three models (Fig. 11). The maximum value is just over 20 Sv (1 Sv $\equiv 10^6$ m^3 s^{-1}) in ESM2G, 22 Sv in MCM-UA, and 26 Sv in ESM2Mb and is found near 40°N. The return flow at depth is slightly shallower in MCM-UA as compared to the two ESMs (noted by the location of the 0-Sv contour). In all three models, there is a weak reverse cell located in the abyssal ocean associated with the circulation of Antarctic Bottom Water (AABW) emanating from the subpolar Southern Ocean.

When the mountains are removed, the AMOC weakens in all three models (Fig. 12). The weakened AMOC leads to cooling in the North Atlantic near the ocean surface as discussed above. In MCM-UA and ESM2G the AMOC weakening is focused on the northern North Atlantic (Fig. 12). In both models, the maximum overturning weakens about 6 Sv (about a 27%–30% reduction). In ESM2G, there is a weakening of the flow at all latitudes, while in MCM-UA the weakening is confined to the NH. Only the MCM-UA is in a near-equilibrium state as discussed in detail in section 3a. The ESM2G NOMTN integration may be close to equilibrium, but the CONTROL integration is still in a transient state. The AMOC weakening in ESM2Mb is quite different from the other two models and is relatively large (more than 10 Sv). Like ESM2G, the weakening extends throughout all latitudes in the Atlantic. The ESM2Mb panel shows the time averages at model years 401–500 for both the CONTROL and NOMTN integrations. The much larger AMOC response in ESM2Mb relative to the other two models is likely a result of the fact that 401–500 years is much too short for an equilibrium response, suggesting that the AMOC is slowly adjusting to the mountains being removed. It is unclear what the equilibrium response of

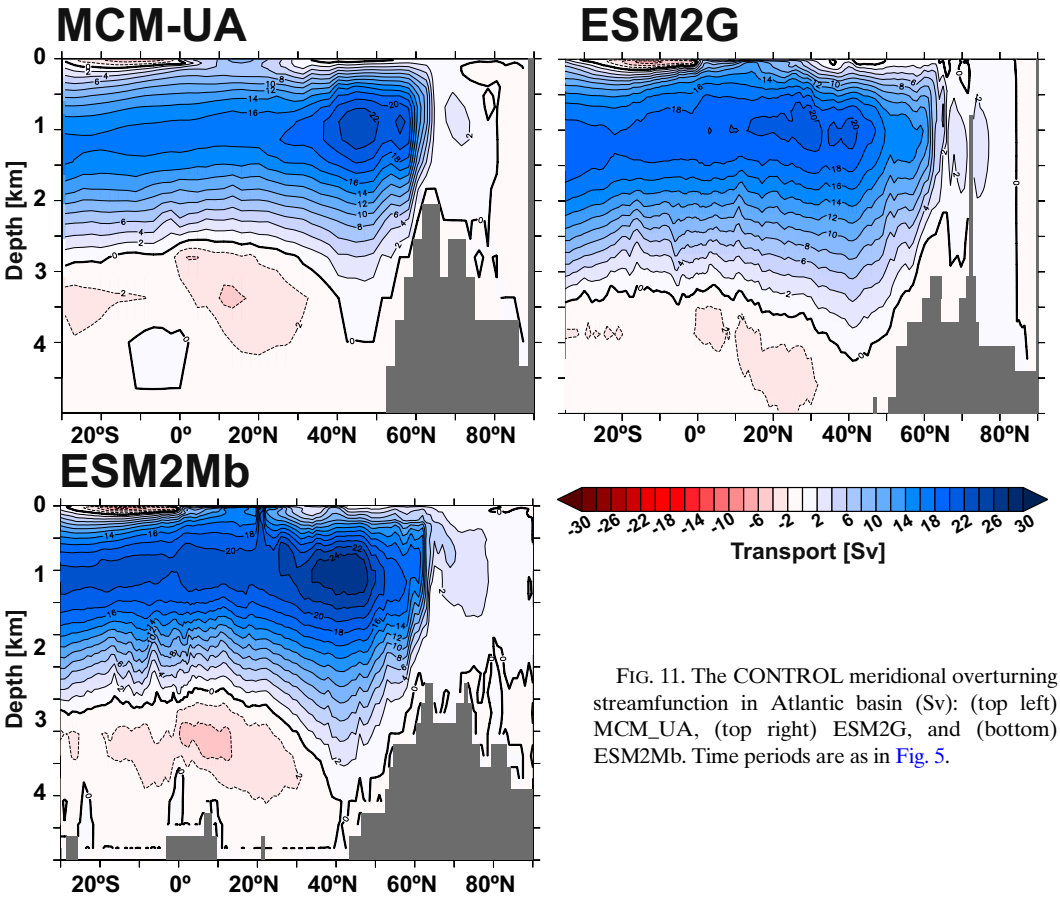

FIG. 11. The CONTROL meridional overturning streamfunction in Atlantic basin (Sv): (top left) MCM_UA, (top right) ESM2G, and (bottom) ESM2Mb. Time periods are as in Fig. 5.

the AMOC would be when the mountains are removed in this model. As discussed above, the cooling in the northern North Atlantic is a little larger in ESM2Mb than in the other two models, which is likely linked to this larger AMOC reduction.

The AMOC weakening is a consequence of the altered momentum and buoyancy fluxes at the ocean surface as a result of the mountain removal. The surface wind stress and wind stress curl fields become more zonal as the wind field becomes more zonally aligned across the Atlantic. This hinders the near-surface northward flow due to Ekman forcing, reducing the meridional penetration of warm, saline subtropical water into the subpolar North Atlantic. The reduced northward penetration of saline subtropical waters reduces the near-surface salinity in the model's deep-water formation regions, hindering the deep-water formation and weakening the AMOC.

The buoyancy fluxes into the ocean are also impacted when the mountains are removed (Tables 1–3). The heat flux changes in the North Atlantic vary among the models with less heat coming out of the ocean in MCM-UA in the NOMTN integration while the ESMs have more heat coming out of the ocean in this region (Table 1). Inspection of the surface heat flux maps (not shown) indicates that all three models have *less* heat coming out of the North Atlantic Ocean on the western side of the basin in the NOMTN integration and *more* heat coming out of the ocean on the eastern side of the basin. Therefore, the sign of net heat flux difference may be positive or negative depending on the exact details of the changes.

The changes in the net water flux over the North Atlantic are more consistent among the models (Table 2), with all three models exhibiting an increase in net surface water flux into this region when the mountains are removed. This increase in surface water flux into the North Atlantic is mostly attributable to large enhancements of river runoff. This enhanced land runoff response in the high northern latitudes was also documented by Broccoli and Manabe (1992) in their mountain removal experiments. Removing the mountains have two closely related impacts to the atmospheric moisture transport into the continental interior. One impact is the increased zonal alignment of the winds increases the moisture transport to the interior. Also, mountains act to block moisture transport into the interior by causing uplift of the air and precipitation on the upwind side of the mountains which dries the air downstream side of the mountains. Thus, removing the mountains increases the amount of moisture reaching the continental interior. As a result, the exact area chosen (whole Arctic and North Atlantic basin or just the region chosen here) does not impact the conclusion that the net water flux into the Atlantic increases in the NOMTN integration relative to the CONTROL and that river runoff is the main driver of this change (Table 3). This enhanced freshwater flux and the

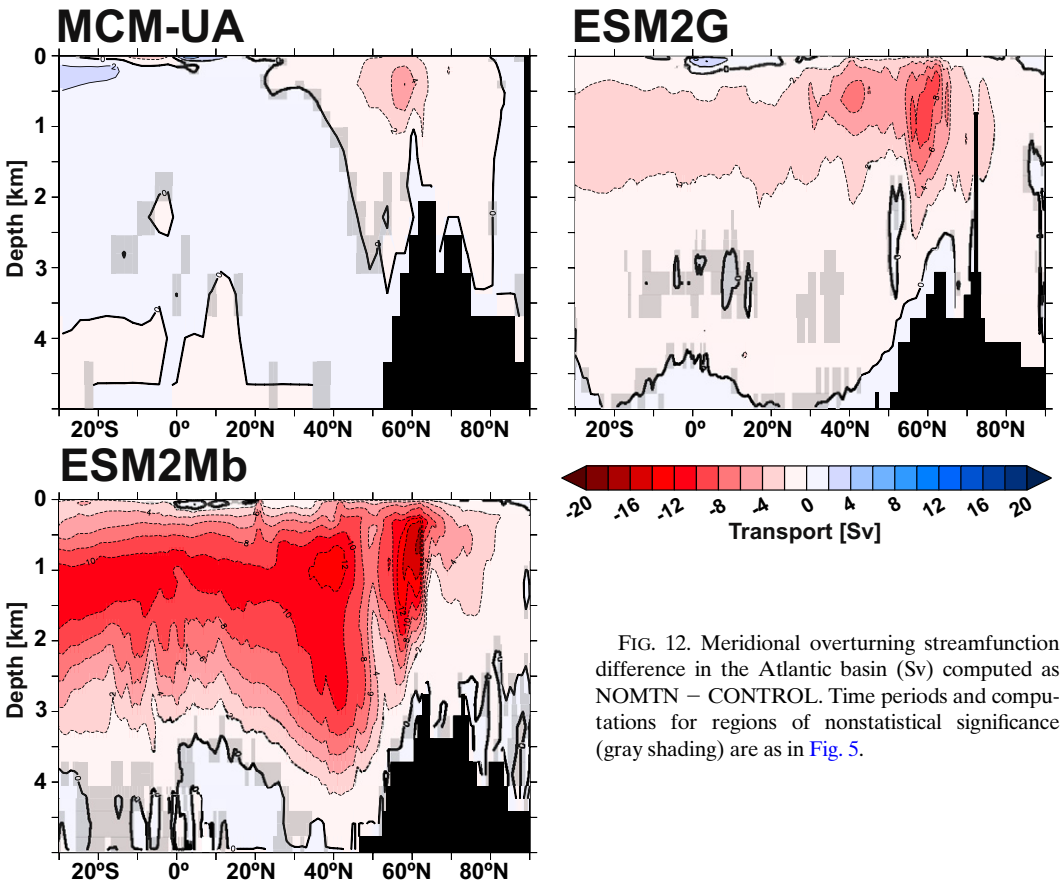

FIG. 12. Meridional overturning streamfunction difference in the Atlantic basin (Sv) computed as NOMTN − CONTROL. Time periods and computations for regions of nonstatistical significance (gray shading) are as in Fig. 5.

increased zonal alignment of the wind stress field in the North Atlantic inhibit oceanic deep convection in the subpolar Atlantic Ocean, weakening the AMOC in all three models in the NOMTN integrations.

f. *Putting the climate response of mountain removal in context of 4xCO_2 simulations*

Despite similar AMOC and surface responses, the models produced fairly different temperature and salinity anomalies in the ocean interior. To put the magnitude of the changes we found with mountain removal in context of other important climate forcings, we compare the NOMTN simulations to the climate response due to a quadrupling of atmospheric CO_2 concentrations (4xCO_2). Using the same ESMs as this study, Krasting et al. (2018) compared the equilibrium response in 4xCO_2 experiments. The ESMs were time integrated for 5000 model years. Using MCM-UA, we performed a similar 4xCO_2 experiment which was integrated for 5500 model years.

The near-equilibrium zonally averaged SST response when atmospheric CO_2 is quadrupled relative to its preindustrial concentration is similar in magnitude and pattern in the three models (Fig. 13). The SST warming is about 5°C from 40°S to 40°N latitude. The MCM-UA warming is larger than ESM2G and ESM2Mb at high latitudes in both hemispheres, implying a larger polar amplification in the MCM-UA. The interior ocean temperature changes in the 4xCO_2 experiments are also similar in pattern and magnitude across models (Fig. 14). All models have enhanced warming in the upper 1500 m and less warming at depth across most latitudes.

Comparing the ocean temperature changes when the mountains are removed (Fig. 9) with the changes due to

TABLE 1. Net surface heat flux (PW; positive values heat the ocean) into the ocean in the North Atlantic Ocean (averaged over 100°W–30°E, 45°N–70°N).

	CONTROL	NOMTN
MCM-UA	−0.0886	−0.1458
ESM2G	−0.5638	−0.4702
ESM2Mb	−0.5720	−0.3487

TABLE 2. Net surface water flux (Sv; positive values add water to the ocean) into the ocean in the North Atlantic (100°W–30°E, 45°–70°N). The net water flux in MCM_UA includes the water flux adjustment term (−0.317 Sv).

	CONTROL	NOMTN
MCM-UA	0.1117	0.1224
ESM2G	0.2705	0.3732
ESM2Mb	0.2836	0.3846

TABLE 3. Net surface water flux components (Sv) into the ocean (same region as in Table 2). Precipitation and evaporation are computed only over the ocean grid points. River runoff computed at the river mouth.

Water flux components (Sv)	Precipitation	Evaporation	River runoff
MCM-UA			
NOMTN	0.321	−0.145	0.375
CONTROL	0.304	−0.160	0.285
ESM2G			
NOMTN	0.269	−0.148	0.253
CONTROL	0.269	−0.152	0.154
ESM2MB			
NOMTN	0.298	−0.166	0.252
CONTROL	0.268	−0.157	0.173

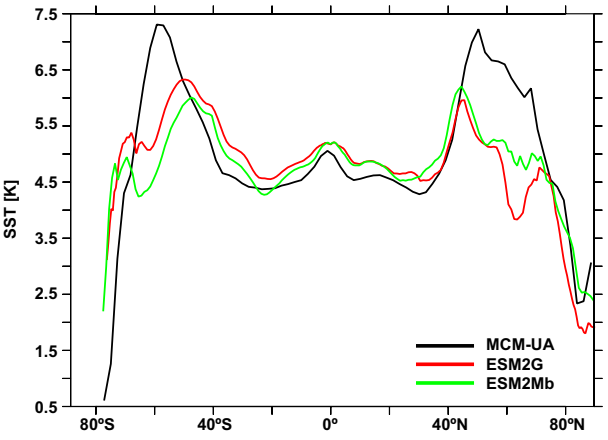

FIG. 13. Zonally averaged sea surface temperature difference (°C) near equilibrium computed as 4xCO_2 minus CONTROL (100-yr time averages at equilibrium).

increased atmospheric CO_2 (Fig. 14), it is noted that the changes associated with increased CO_2 are of one sign (warming) and large, while the changes associated with mountains removal include both warming and cooling and are relatively small in magnitude. One could argue that increasing the atmospheric CO_2 concentration by 4 times is unrealistically large. Given that a doubling of the CO_2 results in about half the radiative forcing, dividing the changes in Fig. 14 by two still leads to the same conclusion in most regions outside of the Arctic interior ocean, namely that the oceanic changes associated with removing the mountains are relatively small but reveal complex interactions between changes in surface forcing, AMOC changes, and interior ocean changes.

The comparison of changes due to increased CO_2 with changes resulting from removing the mountains should also consider the ocean circulation differences as well as the temperature response. To address that issue, we look at changes in a dynamical quantity, the barotropic streamfunction, in the NOMTN and 4xCO_2 forcings (Fig. 15). When the mountains are removed, the subtropical gyre in the Pacific tends to move northward, weakening the Pacific subpolar gyre. This shift is consistent with the northward shift in the wind stress and wind stress curl discussed earlier. In the Atlantic, the subpolar gyre slightly strengthens in MCM-UA, while it weakens in the ESMs. In all the models, the NH subtropical gyre shifts slightly toward the north and the subtropical–subpolar boundary tends to become more zonally aligned. Again, this is consistent with the winds becoming more zonal. In ESM2Mb, the subtropical gyre in the Atlantic weakens much more than in MCM-UA and ESM2G, which is consistent with the smaller AMOC changes in these two models. Near 60°S between 100°E and 160°W, the ACC increases at most longitudes (Fig. 15, second and third rows) when the mountains are removed. In the South Atlantic and western south Indian Ocean basins, the ACC changes differ among the three models.

When CO_2 is quadrupled, the ACC weakens in MCM-UA except for a small region south of Australia and just east of the tip of South America (Figs. 15j,m), while the ACC gets much stronger in the ESMs (Figs. 15k,l,n,o). However, outside of the Southern Ocean, in most regions of the global ocean, the ocean circulation changes due to removing the mountains are comparable in magnitude to those found in the 4xCO_2 simulations. This is in sharp contrast to the interior oceanic temperature changes shown above, which are very different in pattern and magnitude between the NOMTN and 4xCO_2 forcings.

4. Discussion

Given the similarity of the atmospheric and surface flux response to removing the mountains and the previously published demonstration of the similarity of the ESM2Mb and ESM2G responses to a large increase in atmospheric CO_2 concentration (Krasting et al. 2018), our expectation as noted earlier was that the oceanic response would also be similar among the models. The near-surface changes and the AMOC response is generally consistent with this expectation. However, the thermal and haline responses in the ocean interior to mountain removal are different across the three models. Why are the interior ocean anomalies in such disagreement across the three models despite similar surface and AMOC responses?

One contributing factor is that the magnitude of the interior ocean response when the mountains are removed is relatively small in comparison to the models' response to other climate forcing changes such as increased atmospheric CO_2. The relatively small NOMTN response may be related to the fact that the high-latitude forcing has positive and negative regions that compensate for one another. In the case of increased CO_2, the response tends to be of one sign (warming and wetting) at high latitudes. This implies that relatively small changes from model to model when the mountains are removed will have the potential to lead to quite different responses in the ocean interior.

A second reason is that given the relatively small interior oceanic changes, the ocean mixing parameterizations and differences in the CONTROL climates among the models can also lead to different oceanic interior responses. For example, the vertical stability of the World Ocean is much different in ESM2Mb CONTROL when compared to MCM-UA and ESM2G CONTROL integrations (Fig. 16). As noted earlier, ESM2Mb integrations are likely farther from equilibrium

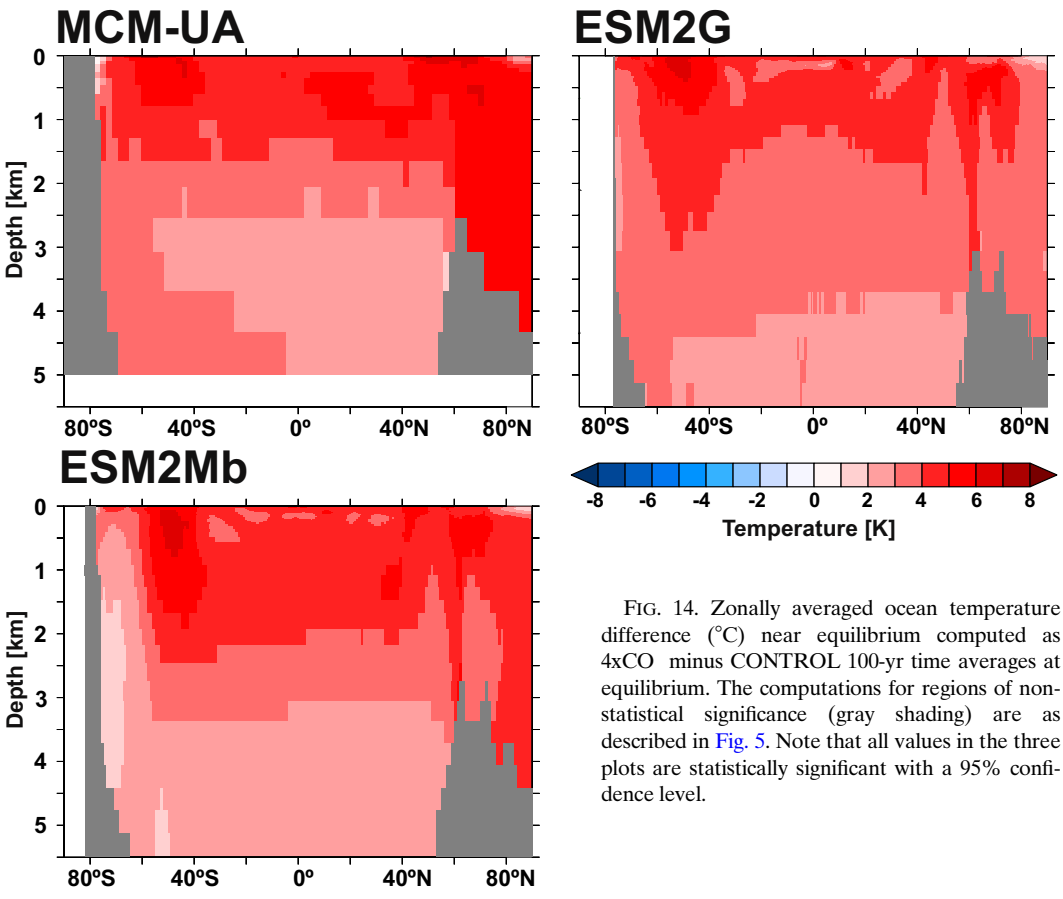

FIG. 14. Zonally averaged ocean temperature difference (°C) near equilibrium computed as 4xCO$_2$ minus CONTROL 100-yr time averages at equilibrium. The computations for regions of nonstatistical significance (gray shading) are as described in Fig. 5. Note that all values in the three plots are statistically significant with a 95% confidence level.

than the others, which can cause differences in the response especially away from the ocean surface. In all three models, the surface temperature is close to the observations in most regions (Figs. 16 and 2). Farther down in the water column (500–1500-m depth), the thermocline in MCM-UA is too diffuse in both basins, a common problem for this generation model. In the Pacific, both ESM thermoclines are close to the observed strength. However, in the Atlantic, the thermocline in ESM2Mb is also too diffuse. Near the ocean bottom in the CONTROL integrations of ESM2G and MCM-UA, the water temperature is within a few degrees of the observations, while it is much warmer in ESM2Mb (Figs. 2 and 16). In fact, ESM2Mb is too warm compared to observations below about 500 m. These results indicate that the stability of the ocean differs across the models, which can impact vertical mixing in the model, leading to different interior oceanic responses to relatively small forcing changes. A similar argument for explaining the different responses can be made for differences in the subgrid-scale mixing parameterizations among the models.

5. Summary

Using an idealized experimental design, we investigate the impact of removing all the mountains on the present-day climate and ocean state using three climate models spanning multiple generations. The atmospheric response in the three models is consistent with that found in previous studies. The atmospheric jet becomes more zonal, particularly in the NH, and the midlatitude rain belts become more zonal, narrow, and intense. In response to removing the mountains, the AMOC weakens in all three models due to the relatively large increase in river discharge in the high latitudes of the North Atlantic. Additionally, the enhanced zonal alignment of the winds in the North Atlantic hinders the near-surface northward flow of subtropical water into the subpolar North Atlantic, reducing the meridional penetration of warm and saline water into regions of deep-water formation. As a result of the AMOC changes, the SSTs cool by about 6°C in the subpolar North Atlantic. These AMOC changes are similar to that found by Fallah et al. (2016), who removed the Tibetan Plateau and found that the AMOC weakened. In the Kuroshio Extension region in the North Pacific, the SSTs in all three models warm. This is a result of the winds shifting northward over the Pacific, allowing the subtropical gyre waters to penetrate farther northward.

The interior oceanic response in terms of temperature and salinity is surprisingly small (though mainly statistically significant at the 95% confidence level), especially when compared to other climate forcings such as increased atmospheric CO_2 concentration. Given the relatively small oceanic interior

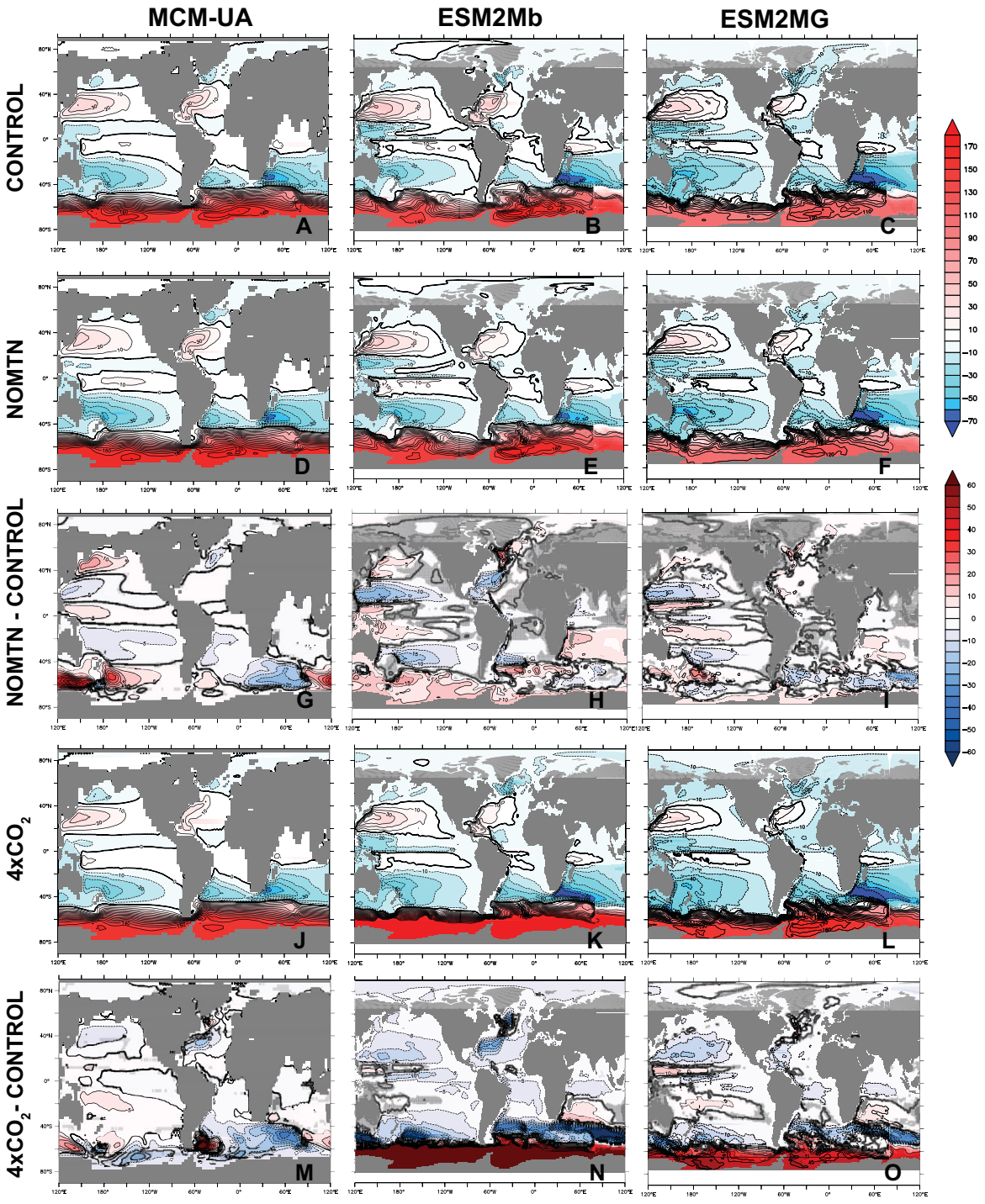

FIG. 15. Barotropic streamfunction (Sv). ESM2Mb data are quasi-barotropic streamfunction (see center column). On time scales longer than 1 year, the quasi-barotropic streamfunction is very close to the barotropic streamfunction. ESM2G data are the mass transport vertically summed and cumulatively summed in the north–south direction. (a)–(c) 100-yr time averages from the CONTROL integrations: MCM-UA years 2101–200, ESM2Mb years 401–500, and ESM2G years 901–1000. (d)–(f) NOMNT; MCM-UA years 1801–900, ESM2Mb years 401–500, and ESM2G years 901–1000. (g)–(i) Differences of NOMNT minus CONTROL; averaging periods for the differences are as detailed above. (j)–(l) $4xCO_2$ MCM-UA years 5501–600 and ESM2Mb and ESM2G years 4901–5000. (m)–(o) Differences for $4xCO_2$ equilibrium minus CONTROL; averaging periods are as in (j)–(l). Note that (a)–(f) and (j)–(l) share the same color bar; also (g)–(i) and (m)–(o) share the same color bar. The computations for regions of nonstatistical significance (gray shading) on the difference panels are as described in Fig. 5.

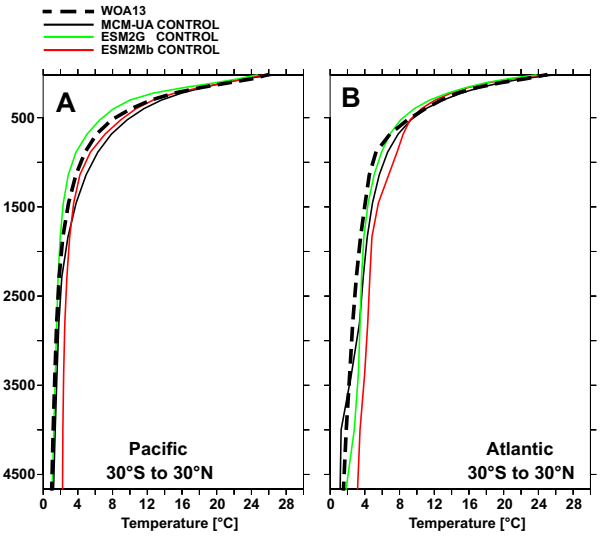

FIG. 16. Ocean temperature with depth (°C) averaged over 30°S–30°N: (a) Pacific and (b) Atlantic. Thick dashed black line are values from the *WOA13* product (Boyer et al. 2013). Thin black line: MCM-UA. Green line: ESM2G. Red line: ESM2Mb. Time periods for the model values are the same as in Fig. 5.

changes when the mountains are removed, it is not surprising that the difference patterns in ocean properties found in the three models are different from each other.

The dynamical ocean response to removing the mountains, as shown by the barotropic streamfunction changes, is of a similar magnitude to the changes associated with changes due to increased CO_2. This is somewhat surprising since the radiative forcing associated with the CO_2 changes results in large changes in density. However, it is the *density gradients* that drive ocean circulation, and these gradients do not change very much at equilibrium in response to the $4xCO_2$ forcing for much of the global ocean. One may assume that the density and ocean circulation changes are tightly coupled on time scales longer than a year or so. Here we show this is not always the case. This contributed to our having partially falsified our initial hypothesis that the ocean responses would be quite similar among the models. In general, only the ocean interior responses vary among the models.

The main takeaway is that the removal of mountains has a large impact on climate near the ocean surface and for the AMOC. The impact on the ocean interior from a mean density field perspective is not as large. However, the oceanic *density gradients*, which drive the large-scale ocean circulation patterns, do change, so one must be aware of this point when studying past oceanic changes. Also, this result does not suggest that the mountains or their location are unimportant to defining the ocean mean state. The ocean interior is in contact with the atmosphere only in a few regions, mainly found in high latitudes. It is possible that removing one or more of the high-latitude mountains may have larger impacts than found when removing all the mountains as in the idealized case presented here.

There are many caveats associated with this study. The main one is related to the relatively low model resolution used here. Such models are known to have problems simulating atmospheric teleconnections (Stoner et al. 2009). Given that the mountains greatly influence the pattern and magnitude of the teleconnections, the ocean response could be quite different using a model where these teleconnections are better simulated. A related issue is that the precise locations of the important deep-water formation regions are resolution and model dependent. In the ocean components, none of the models presented here resolve the mixing associated with eddies and other subgrid-scale processes (such as tides). They incorporate subgrid-scale mixing schemes to accomplish the unresolved mixing. These subgrid-scale schemes can have a large impact on the simulation of ocean phenomena such as boundary currents and vertical mixing. As a result, these mixing schemes can impact the response to perturbations (e.g., removing topography). In light of these various caveats, the results must be viewed with caution.

An interesting question raised by this study, but not directly addressed, is the role of flux adjustments in the MCM-UA response. The use of flux adjustments greatly improved the simulation of the surface climate in MCM-UA and reduced the model's climate drift (Delworth et al. 2002). The brief analysis presented here indicates that the MCM-UA simulated errors are generally larger in the interior ocean than the ESMs but not so large as to make the results suspect. The MCM-UA oceanic volume averaged temperature and vertical temperature structure are closer to the observed value than found in ESM2Mb. The precipitation simulation in the tropical Pacific is also more realistic given the much smaller SH ITCZ in MCM-UA. In the end, the response of MCM-UA to both removing the mountains and to increased CO_2 is not completely dissimilar to the ESMs. We believe its inclusion provides more insight into the changes we found.

This is an idealized study where we have made several important assumptions in the experimental design. Besides flattening all the world's topography, we did not change the ocean bathymetry and the river drainage map. Both of these assumptions, if modified, could lead to different results. Also, only the MCM-UA is in a near-equilibrium state. The ESM2Mb is clearly not at equilibrium while ESM2G may be close. Unfortunately, computational constraints inhibit these ESMs from being integrated to a near-equilibrium state. Finally, it should be noted that other arrangements of the continents and of the ocean bathymetry can greatly impact the ocean mean state (Bryan 1986; Weaver et al. 2001; Sijp and England 2004).

Acknowledgments. Drs. John P. Dunne and Stephen Griffies and two anonymous reviewers provided very helpful comments on earlier versions of this manuscript. The authors are also grateful for the support of Dr. V. Ramaswamy, Director of GFDL. The HPC support team at UA where the MCM-UA model was integrated was also very helpful. JR and RB: This work was funded by NSF's Southern Ocean Carbon and Climate Observations and Modeling (SOCCOM) Project under NSF Award PLR-1425989, with additional support

from NOAA and NASA. Logistical support for SOCCOM in the Antarctic was provided by the U.S. NSF through the U.S. Antarctic Program. ZN: This work was supported in part by the National Science Foundation (NSF) Frontiers in Earth System Dynamics and NSF Grant EAR-1338553.

REFERENCES

Abe, M., T. Yasunari, and A. Kitoh, 2004: Effects of large-scale orography on the coupled atmosphere–ocean system in the tropical Indian and Pacific Oceans in boreal summer. *J. Meteor. Soc. Japan*, **82**, 745–759, https://doi.org/10.2151/jmsj.2004.745.

Baldwin, J. W., G. A. Vecchi, and S. Bordoni, 2019: The direct and ocean-mediated influence of Asian orography on tropical precipitation and cyclones. *Climate Dyn.*, **53**, 805–824, https://doi.org/10.1007/s00382-019-04615-5.

Barron, E. J., 1985: Explanations of the tertiary global cooling trend. *Palaeogeogr. Palaeoclimatol. Palaeoecol.*, **50**, 45–61, https://doi.org/10.1016/S0031-0182(85)80005-5.

——, and W. Washington, 1984: The role of geographic variables in explaining paleoclimates: Results from Cretaceous climate model sensitivity studies. *J. Geophys. Res.*, **89**, 1267–1279, https://doi.org/10.1029/JD089iD01p01267.

Beadling, R. L., and Coauthors, 2020: Representation of Southern Ocean properties across Coupled Model Intercomparison Project generations: CMIP3 to CMIP6. *J. Climate*, **33**, 6555–6581, https://doi.org/10.1175/JCLI-D-19-0970.1.

Boer, G., 2000: A study of atmosphere–ocean predictability on long time scales. *Climate Dyn.*, **16**, 469–477, https://doi.org/10.1007/s003820050340.

Boos, W. R., and Z. Kuang, 2010: Dominant control of the South Asian monsoon by orographic insulation versus plateau heating. *Nature*, **463**, 218–222, https://doi.org/10.1038/nature08707.

——, and ——, 2013: Sensitivity of the South Asian monsoon to elevated and non-elevated heating. *Sci. Rep.*, **3**, 1192, https://doi.org/10.1038/srep01192.

Boyer, T. P., and Coauthors, 2013: *World Ocean Database 2013*. NOAA Atlas NESDIS 72, 209 pp., https://doi.org/10.7289/V5NZ85MT.

Broccoli, A. J., and S. Manabe, 1992: The effects of orography on midlatitude Northern Hemisphere dry climates. *J. Climate*, **5**, 1181–1201, https://doi.org/10.1175/1520-0442(1992)005<1181:TEOOOM>2.0.CO;2.

——, K. A. Dahl, and R. J. Stouffer, 2006: Response of the ITCZ to Northern Hemisphere cooling. *Geophys. Res. Lett.*, **33**, L01702, https://doi.org/10.1029/2005GL024546.

Bryan, K., 1986: High-latitude salinity effects and interhemispheric thermohaline circulation. *Nature*, **323**, 301–304, https://doi.org/10.1038/323301a0.

Ciais, P., and Coauthors, 2013: Carbon and other biogeochemical cycles. *Climate Change 2013: The Physical Science Basis*, T. F. Stocker et al., Eds., Cambridge University Press, 465–570, https://doi.org/10.1017/CBO9781107415324.015.

Collins, M., and Coauthors, 2013: Long-term climate change: Projections, commitments and irreversibility. *Climate Change 2013: The Physical Science Basis*, T. F. Stocker et al., Eds., Cambridge University Press, 1029–1136.

Cubasch, U., and Coauthors, 2001: Projections of future climate change. *Climate Change 2001: The Scientific Basis*, Cambridge University Press, 526–582.

Delworth, T. L., R. Stouffer, K. Dixon, M. Spelman, T. Knutson, A. Broccoli, P. Kushner, and R. Wetherald, 2002: Review of simulations of climate variability and change with the GFDL R30 coupled climate model. *Climate Dyn.*, **19**, 555–574, https://doi.org/10.1007/s00382-002-0249-5.

Dunne, J. P., and Coauthors, 2012: GFDL's ESM2 global coupled climate–carbon Earth system models. Part I: Physical formulation and baseline simulation characteristics. *J. Climate*, **25**, 6646–6665, https://doi.org/10.1175/JCLI-D-11-00560.1.

——, and Coauthors, 2013: GFDL's ESM2 global coupled climate–carbon Earth system models. Part II: Carbon system formulation and baseline simulation characteristics. *J. Climate*, **26**, 2247–2267, https://doi.org/10.1175/JCLI-D-12-00150.1.

Fallah, B., U. Cubasch, K. Pömmel, and S. Sodoudi, 2016: A numerical model study on the behaviour of Asian summer monsoon and AMOC due to orographic forcing of Tibetan Plateau. *Climate Dyn.*, **47**, 1485–1495, https://doi.org/10.1007/s00382-015-2914-5.

Feng, R., and C. J. Poulsen, 2014: Andean elevation control on tropical Pacific climate and ENSO. *Climate Dyn.*, **47**, 1485–1495, https://doi.org/10.1007/s00382-015-2914-5.

Gebbie, G., and P. Huybers, 2019: The Little Ice Age and 20th-century deep Pacific cooling. *Science*, **363**, 70–74, https://doi.org/10.1126/science.aar8413.

Hallberg, R., 1995: Some aspects of the circulation in ocean basins with isopycnals intersecting the sloping boundaries. Ph.D. thesis, University of Washington, 244 pp. [Available from University Microfilms, 1490 Eisenhower Place, P.O. Box 975, Ann Arbor, MI 48106.]

Kitoh, A., 1997: Mountain uplift and surface temperature changes. *Geophys. Res. Lett.*, **24**, 185–188, https://doi.org/10.1029/96GL03953.

——, 2004: Effects of mountain uplift on East Asian summer climate investigated by a coupled atmosphere–ocean GCM. *J. Climate*, **17**, 783–802, https://doi.org/10.1175/1520-0442(2004)017<0783:EOMUOE>2.0.CO;2.

——, 2007: ENSO modulation by mountain uplift. *Climate Dyn.*, **28**, 781–796, https://doi.org/10.1007/s00382-006-0209-6.

Krasting, J. P., R. J. Stouffer, S. M. Griffies, R. W. Hallberg, S. L. Malyshev, B. L. Samuels, and L. T. Sentman, 2018: Role of ocean model formulation in climate response uncertainty. *J. Climate*, **31**, 9313–9333, https://doi.org/10.1175/JCLI-D-18-0035.1.

Kutzbach, J. E., and P. Guetter, 1989: Sensitivity of climate to late Cenozoic uplift in Southern Asia and the American West: Numerical experiments. *J. Geophys.*, **94**, 18 393–18 407, https://doi.org/10.1029/JD094iD15p18393.

——, W. L. Prell, and W. F. Ruddiman, 1993: Sensitivity of Eurasian climate to surface uplift of the Tibetan Plateau. *J. Geol.*, **101**, 177–190, https://doi.org/10.1086/648215.

Lee, J.-Y., B. Wang, K.-H. Seo, K.-J. Ha, A. Kitoh, and J. Liu, 2015: Effects of mountain uplift on global monsoon precipitation. *Asia-Pac. J. Atmos. Sci.*, **51**, 275–290, https://doi.org/10.1007/s13143-015-0077-2.

Lin, J. L., 2007: The double-ITCZ problem in IPCC AR4 coupled GCMs: Ocean–atmosphere feedback analysis. *J. Climate*, **20**, 4497–4525, https://doi.org/10.1175/JCLI4272.1.

Lutsko, N. J., J. W. Baldwin, and T. W. Cronin, 2019: The impact of large-scale orography on Northern Hemisphere winter synoptic temperature variability. *J. Climate*, **32**, 5799–5814, https://doi.org/10.1175/JCLI-D-19-0129.1.

Manabe, S., and T. B. Terpstra, 1974: The effects of mountains on the general circulation of the atmosphere as identified by numerical experiments. *J. Atmos. Sci.*, **31**, 3–42, https://doi.org/10.1175/1520-0469(1974)031<0003:TEOMOT>2.0.CO;2.

——, and R. J. Stouffer, 1988: Two stable equilibria of a coupled ocean–atmosphere model. *J. Climate*, **1**, 841–866, https://doi.org/10.1175/1520-0442(1988)001<0841:TSEOAC>2.0.CO;2.

——, and A. Broccoli, 1990: Mountains and arid climates of middle latitudes. *Science*, **247**, 192–195, https://doi.org/10.1126/science.247.4939.192.

——, R. J. Stouffer, M. J. Spelman, and K. Bryan, 1991: Transient responses of a coupled ocean–atmosphere model to gradual changes of atmospheric CO_2. Part I: Annual mean response. *J. Climate*, **4**, 785–818, https://doi.org/10.1175/1520-0442(1991)004<0785:TROACO>2.0.CO;2.

Maroon, E., D. M. W. Frierson, and D. S. Battisti, 2015: The tropical precipitation response to Andes topography and ocean heat fluxes in an aquaplanet model. *J. Climate*, **28**, 381–398, https://doi.org/10.1175/JCLI-D-14-00188.1.

Matsumoto, K., 2007: Radiocarbon-based circulation age of the world oceans. *J. Geophys. Res.*, **112**, C09004, https://doi.org/10.1029/2007JC004095.

Naiman, Z., P. J. Goodman, J. P. Krasting, S. L. Malyshev, J. L. Russell, R. J. Stouffer, and A. T. Wittenberg, 2017: Impact of mountains on tropical circulation in two Earth system models. *J. Climate*, **30**, 4149–4163, https://doi.org/10.1175/JCLI-D-16-0512.1.

Pacanowski, R. C., K. W. Dixon, and A. Rosati, 1991: The GFDL modular ocean model users guide. GFDL Ocean Group Tech. Rep. 2, 46 pp., https://mom-ocean.github.io/assets/pdfs/MOM1_manual.pdf.

Schmittner, A., T. M. Silva, K. Fraedrich, E. Kirk, and F. Lunkeit, 2011: Effects of mountains and ice sheets on global ocean circulation. *J. Climate*, **24**, 2814–2829, https://doi.org/10.1175/2010JCLI3982.1.

Schneider, T., T. Bischoff, and G. H. Haug, 2014: Migrations and dynamics of the intertropical convergence zone. *Nature*, **513**, 45–53, https://doi.org/10.1038/nature13636.

Sijp, W. P., and M. H. England, 2004: Effect of the Drake Passage throughflow on global climate. *J. Phys. Oceanogr.*, **34**, 1254–1266, https://doi.org/10.1175/1520-0485(2004)034<1254:EOTDPT>2.0.CO;2.

Singh, H. K. A., C. M. Bitz, and D. M. W. Frierson, 2016: The global climate response to lowering surface orography of Antarctica and the importance of atmosphere–ocean coupling. *J. Climate*, **29**, 4137–4153, https://doi.org/10.1175/JCLI-D-15-0442.1.

Sinha, B., A. T. Blaker, J. J. M. Hirschi, S. Bonham, M. Brand, S. Josey, R. S. Smith, and J. Marotzke, 2012: Mountain ranges favour vigorous Atlantic meridional overturning. *Geophys. Res. Lett.*, **39**, L02705, https://doi.org/10.1029/2011GL050485.

Stoner, A. M. K., K. Hayhoe, and D. J. Wuebbles, 2009: Assessing circulation models of atmospheric teleconnection patterns. *J Climate*, **22**, 4348–4372, https://doi.org/10.1175/2009JCLI2577.1.

Takahashi, K., and D. S. Battisti, 2007a: Processes controlling the mean tropical Pacific precipitation pattern. Part I: The Andes and the eastern Pacific ITCZ. *J. Climate*, **20**, 3434–3451, https://doi.org/10.1175/JCLI4198.1.

——, and ——, 2007b: Processes controlling the mean tropical Pacific precipitation pattern. Part II: The SPCZ and the southeast Pacific dry zone. *J. Climate*, **20**, 5696–5706, https://doi.org/10.1175/2007JCLI1656.1.

Thiele, G., and J. L. Sarmiento, 1990: Tracer dating and ocean ventilation. *J. Geophys. Res.*, **95**, 9377–9391, https://doi.org/10.1029/JC095iC06p09377.

Weaver, A. J., and Coauthors, 2001: The UVic Earth System Climate Model: Model description, climatology and applications to past, present and future climates. *Atmos.–Ocean*, **39**, 361–428, https://doi.org/10.1080/07055900.2001.9649686.

Xu, H., Y. Wang, and S. P. Xie, 2004: Effects of the Andes on eastern Pacific climate: A regional atmospheric model study. *J. Climate*, **17**, 589–602, https://doi.org/10.1175/1520-0442(2004)017<0589:EOTAOE>2.0.CO;2.

Zanna, L., S. Khatiwala, J. M. Gregory, J. Ison, and P. Heimbach, 2019: Global reconstruction of the historical ocean heat storage and transport. *Proc. Natl. Acad. Sci. USA*, **116**, 1126–1131, https://doi.org/10.1073/pnas.1808838115.